nature neuroscience

Rett syndrome mutation MeCP2 T158A disrupts DNA binding, protein stability and ERP responses

Darren Goffin[1], Megan Allen[1,5], Le Zhang[1,5], Maria Amorim[1,5], I-Ting Judy Wang[1,5], Arith-Ruth S Reyes[1], Amy Mercado-Berton[2], Caroline Ong[3], Sonia Cohen[3], Linda Hu[3], Julie A Blendy[2], Gregory C Carlson[4], Steve J Siegel[4], Michael E Greenberg[3] & Zhaolan Zhou[1]

Mutations in the *MECP2* gene cause the autism spectrum disorder Rett syndrome (RTT). One of the most common MeCP2 mutations associated with RTT occurs at threonine 158, converting it to methionine (T158M) or alanine (T158A). To understand the role of T158 mutations in the pathogenesis of RTT, we generated knockin mice that recapitulate the MeCP2 T158A mutation. We found a causal role for T158A mutation in the development of RTT-like phenotypes, including developmental regression, motor dysfunction, and learning and memory deficits. These phenotypes resemble those present in *Mecp2* null mice and manifest through a reduction in MeCP2 binding to methylated DNA and a decrease in MeCP2 protein stability. The age-dependent development of event-related neuronal responses was disrupted by MeCP2 mutation, suggesting that impaired neuronal circuitry underlies the pathogenesis of RTT and that assessment of event-related potentials (ERPs) may serve as a biomarker for RTT and treatment evaluation.

RTT is an autism spectrum disorder that is caused by mutations in the X-linked gene encoding methyl-CpG binding protein 2 (MeCP2)[1]. RTT is associated with different types of mutations in *MECP2*, including missense, nonsense, deletions and insertions[2]. Individuals with classical RTT, irrespective of the type of mutation, develop normally for the first 6–18 months of age, after which they enter a period of regression that is characterized by deceleration of head growth and a loss of acquired motor and language skills. Frequently, affected individuals develop stereotypic hand wringing, abnormal breathing, seizures and autistic behaviors[3]. The molecular mechanisms through which different types of *MECP2* mutations lead to disruptions in proper brain function are not fully understood.

Mice engineered with different *Mecp2* alterations have phenotypes that are both similar and distinct from those observed in *Mecp2* null mice[4–11]. These similarities and differences in mouse models suggest that different *MECP2* mutations are likely to have both shared and distinct biochemical and physiological correlates. Notably, reintroduction of MeCP2 into behaviorally affected *Mecp2* null mice is sufficient to rescue RTT-like phenotypes[12], and restoration of MeCP2 function in astrocytes alone substantially improves the developmental outcome of *Mecp2*$^{-/y}$ mice[13], suggesting that RTT is reversible after restoration of MeCP2 function. Thus, understanding the mechanisms by which different MeCP2 mutations lead to RTT may reveal effective strategies that are tailored to the particular mutation to restore MeCP2 function.

Mutation of the T158 residue, located at the C terminus of the methyl-CpG binding domain (MBD) of MeCP2, represents one of the most common mutations observed in RTT. Approximately 10% of all RTT cases carry a single nucleotide mutation converting T158 to methionine (T158M) or, in rare cases, to alanine (T158A)[2]. It has been suggested that the T158 residue is important for the stabilization of the MBD and the binding of MeCP2 to methylated DNA[14]. Whether mutation of T158 leads to MeCP2 gain-of-function or loss-of-function, however, is not clear.

The onset of RTT symptoms occurs during the establishment and refinement of neural networks in early postnatal development. Studies in *Mecp2* null mice have suggested that reductions in connectivity between excitatory pyramidal neurons are associated with RTT-like phenotypes[15–17]. The means by which reductions in neuronal connectivity lead to the manifestation of the age-dependent cognitive and behavioral deficits in RTT are currently unknown. Cognitive dysfunctions are frequently assessed by measuring the neurophysiological responses that occur during passive processes or during the performance of cognitive, sensory or motor tasks. Brain activations that occur during these tasks manifest as ERPs. Disruptions in ERPs and the oscillations that underlie them are associated with a number of cognitive disorders, such as schizophrenia[18,19] and autism[20,21]. Electroencephalography (EEG) recordings in *Mecp2*$^{-/y}$ mice[22,23] and ERP recordings in individuals with RTT[24,25] also suggest that alterations in brain activity are associated with behavioral and cognitive deficits. How ERPs are affected by MeCP2 dysfunction and how changes in EEG and ERPs correlate with the age-dependent progression of RTT-like symptoms, however, remain to be determined.

Given the high frequency of T158 mutations in RTT and its role in methyl-DNA binding, we sought to model this mutation *in vivo* and developed knockin mice containing the T158A mutation (*Mecp2*$^{T158A/y}$ mice). We found that these mice recapitulate a number

[1]Department of Genetics, University of Pennsylvania School of Medicine, Philadelphia, Pennsylvania, USA. [2]Department of Pharmacology, University of Pennsylvania School of Medicine, Philadelphia, Pennsylvania, USA. [3]Department of Neurobiology, Harvard Medical School, Boston, Massachusetts, USA. [4]Department of Psychiatry, University of Pennsylvania School of Medicine, Philadelphia, Pennsylvania, USA. [5]These authors contributed equally to this work. Correspondence should be addressed to Z.Z. (zhaolan@mail.med.upenn.edu).

Received 25 July; accepted 28 October; published online 27 November 2011; doi:10.1038/nn.2997

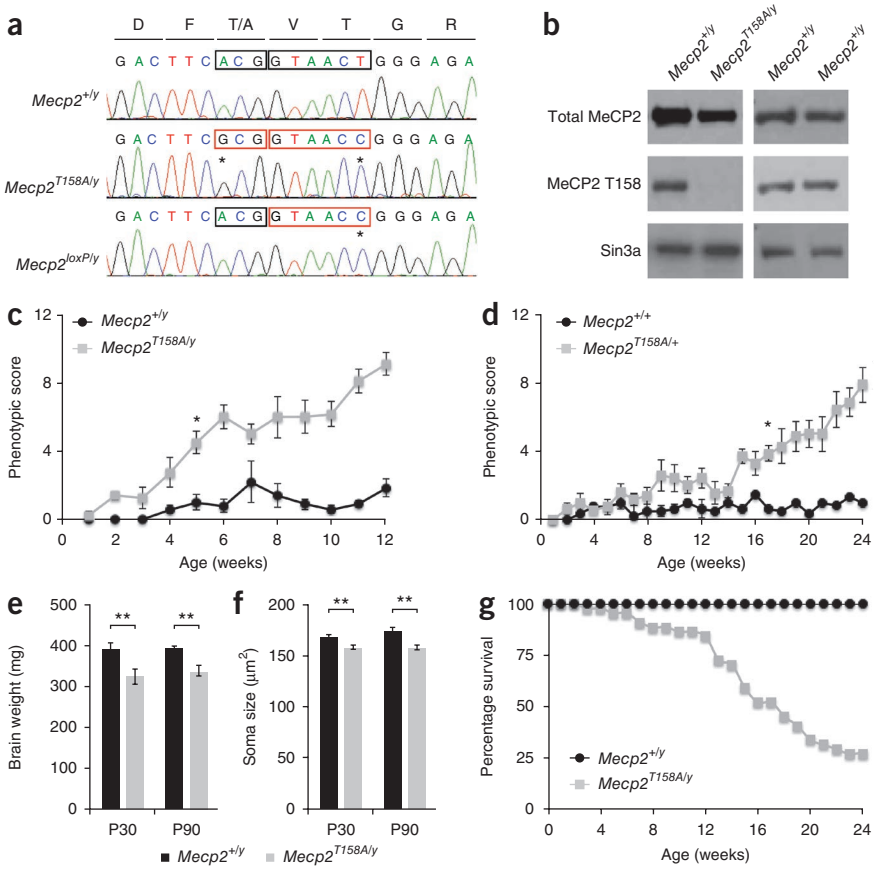

Figure 1 Generation and phenotypic characterization of *Mecp2*$^{T158A/y}$ mice. (**a**) Sequencing chromatogram of RT-PCR products from *Mecp2* mRNA. Mutation of the threonine 158 codon ACG to GCG (alanine, first box) and creation of BstEII restriction site (second box) with a silent mutation are marked with an asterisk. (**b**) Western blots probed with a site-specific MeCP2 T158 antibody, a total MeCP2 antibody and a Sin3a antibody. (**c**) Developmental presentation of RTT-like phenotypes in male *Mecp2*$^{T158A/y}$ mice ($n = 6$, $F_{1,252} = 27.75$, $P < 0.0001$, two-way ANOVA) relative to wild-type littermates ($n = 5$). Symbols represent mean score ± s.e.m. Phenotypic score was significantly higher in *Mecp2*$^{T158A/y}$ mice than in wild-type littermates at 5 weeks and thereafter (*$P < 0.05$, two-way ANOVA with Bonferroni correction). (**d**) Developmental presentation of RTT-like phenotypes in female *Mecp2*$^{T158A/+}$ mice ($n = 7$, $F_{1,224} = 198.6$, $P < 0.0001$, two-way ANOVA) relative to *Mecp2*$^{+/+}$ littermates ($n = 6$). Symbols represent mean score ± s.e.m. Phenotypic score was significantly higher in *Mecp2*$^{T158A/+}$ mice than in wild-type littermates at 17 weeks and thereafter (*$P < 0.05$, two-way ANOVA with Bonferroni correction). (**e**) Brain weights at P30 ($n = 4$ for both genotypes) and P90 ($n = 6$ for both genotypes). Bars represent mean ± s.e.m. **$P < 0.01$, two-tailed *t* test with Bonferroni correction. (**f**) Soma size in hippocampal CA1 pyramidal neurons. Bars represent mean ± s.e.m. ($n = 100$ cells from 5 mice per genotype) asterisks same as in (**e**). (**g**) Survival of male *Mecp2*$^{T158A/y}$ ($n = 43$) and *Mecp2*$^{+/y}$ littermates ($n = 43$).

of RTT-like symptoms observed in *Mecp2* null mice, including late onset of hypoactivity, poor motor control, irregular breathing, altered anxiety, impaired learning and memory, and shortened lifespan. We found that T158A mutation decreased the binding of MeCP2 to methylated DNA *in vitro* and *in vivo*, and reduced MeCP2 protein stability. Moreover, the amplitude and latency of ERPs in both *Mecp2*$^{T158A/y}$ and *Mecp2*$^{-/y}$ mice were substantially altered. Time-frequency analysis of these ERPs revealed that *Mecp2*$^{T158A/y}$ mice failed to show a developmental increase in event-related power and phase locking as compared with wild-type mice, indicating that MeCP2 is required for the development of functional neuronal circuits. Our results suggest that stabilization of MeCP2 protein and enhancement of its affinity for methylated DNA may provide a potential therapeutic approach for treating individuals with a MeCP2 T158 mutation. Furthermore, assessment of ERPs may serve as a biomarker for RTT and the evaluation of therapeutic efficacy in RTT treatment.

RESULTS

Generation of *Mecp2*$^{T158A/y}$ and *Mecp2*$^{loxP/y}$ mice

Although the T158A mutation occurs at a lower frequency than the T158M mutation in individuals with RTT, the mechanism by which both mutations impair MeCP2 function is believed to be the same: the lack of hydroxyl group in alanine and methionine destabilizes the tandem Asx-ST motif in the MBD and thereby reduces MeCP2 affinity for methylated DNA[14]. Indeed, individuals carrying MeCP2 T158A or T158M mutations are phenotypically similar in the identity and severity of presented symptoms[26,27]. To examine the importance of the T158 residue in MeCP2 function, we developed a knockin mouse with a T158A mutation to circumvent the potential steric interference brought about by the larger methionine residue. To facilitate screening of properly targeted embryonic stem (ES) cells, we incorporated a silent mutation at codon 160 to create a new BstEII restriction site and a *loxP*-flanked neomycin expression cassette in intron III of the *Mecp2* gene (**Supplementary Fig. 1**). Given that our goal was to test a rather subtle mutation on MeCP2, a single amino acid change of T158A, we also engineered *loxP* knockin mice (*Mecp2*$^{loxP/y}$), which contained the BstEII restriction site and *loxP* insertion, but lacked the T158A mutation, to rule out the possibility that manipulation of the *Mecp2* locus may affect MeCP2 expression (**Supplementary Fig. 1**).

Sequencing of MeCP2 mRNA extracted from brain tissues of wild-type, *Mecp2*$^{T158A/y}$ and *Mecp2*$^{loxP/y}$ mice verified that both *Mecp2*$^{T158A/y}$ and *Mecp2*$^{loxP/y}$ mice contained the thymine to cytosine mutation at codon 160 for the generation of the BstEII restriction site, whereas only *Mecp2*$^{T158A/y}$ mice contain the adenine to guanine mutation at codon 158 (**Fig. 1a**). Furthermore, a MeCP2 T158 site-specific antibody recognized MeCP2 protein from wild-type and *Mecp2*$^{loxP/y}$ mice, but not from *Mecp2*$^{T158A/y}$ mice, confirming the successful generation of *Mecp2*$^{T158A/y}$ mice (**Fig. 1b**).

Mecp2$^{T158A/y}$ mice recapitulate RTT-like phenotypes

RTT is characterized by relatively normal development during the first 6–18 months of life, followed by a period of developmental stagnation leading to motor impairments, breathing abnormalities and intellectual disability. We evaluated the presence, development and progression of RTT-like phenotypes in MeCP2 T158A mice following a previously reported scoring system[12]. Male *Mecp2*$^{T158A/y}$ mice presented no overt symptoms during the first 4 weeks of life, but became progressively symptomatic after 5 weeks of age, as indicated by an increasing phenotypic score (**Fig. 1c**). The hindlimb clasping apparent in *Mecp2*$^{-/y}$ mice was also observed in *Mecp2*$^{T158A/y}$ mice

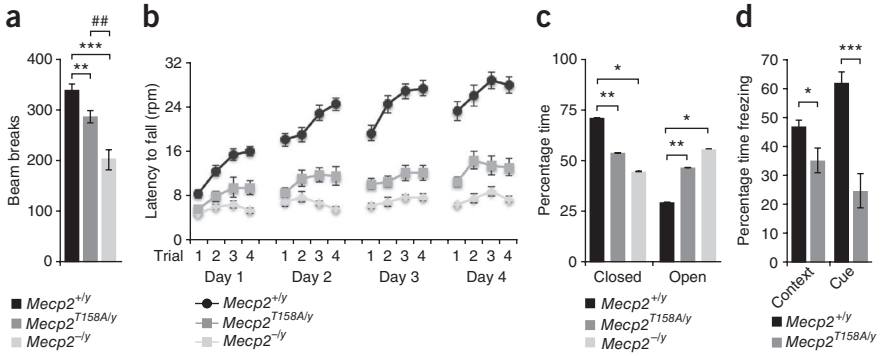

Figure 2 Behavioral characterization of *Mecp2*$^{T158A/y}$ mice. (**a**) Locomotor activity in *Mecp2*$^{T158A/y}$ mice ($n = 15$), *Mecp2*$^{-/y}$ mice ($n = 14$) and *Mecp2*$^{+/y}$ littermates (wild type, $n = 33$) at 9 weeks of age. Bars represent mean ± s.e.m. $^{**}P < 0.01$ and $^{***}P < 0.001$ versus *Mecp2*$^{T158A/y}$, $^{\#\#}P < 0.001$ versus wild type, one-way ANOVA with Tukey's *post hoc* test. (**b**) Motor coordination and motor learning was assessed using a rotarod assay in *Mecp2*$^{T158A/y}$ mice ($n = 16$, $F_{1,645} = 447.2$, $P < 0.0001$, two-way ANOVA) and *Mecp2*$^{-/y}$ mice ($n = 14$, $F_{1,602} = 841.46$, $P < 0.0001$, two-way ANOVA) and *Mecp2*$^{+/y}$ littermates ($n = 27$) at 9 weeks of age. The deficit in *Mecp2*$^{-/y}$ mice was significantly more than that observed in *Mecp2*$^{T158A/y}$ mice ($F_{1,437} = 83.82$, $P < 0.0001$, two-way ANOVA). Symbols represent mean ± s.e.m. (**c**) Anxiety-like behavior in *Mecp2*$^{T158A/y}$ mice ($n = 15$) and *Mecp2*$^{-/y}$ mice ($n = 11$) was measured using elevated zero maze and compared with that of *Mecp2*$^{+/y}$ littermates ($n = 32$) at 9 weeks of age. Bars represent mean ± s.e.m. $^{*}P < 0.05$ and $^{**}P < 0.01$, one-way ANOVA with Tukey's *post hoc* test. (**d**) Learning and memory assessed using context- and cue-dependent fear conditioning in *Mecp2*$^{T158A/y}$ mice ($n = 16$) and *Mecp2*$^{+/y}$ littermates ($n = 33$) at 10 weeks of age. Bars represent mean ± s.e.m. $^{*}P < 0.05$ and $^{***}P < 0.001$, two-tailed *t*-test with Bonferroni correction.

(**Supplementary Fig. 2a**). *Mecp2*$^{T158A/y}$ mice weighed significantly less than their wild-type littermates starting from 4 weeks of age ($P < 0.0001$), but then gradually gained weight until they reached wild-type levels at 8 weeks of age (**Supplementary Fig. 2b**). In contrast, the body weights of *Mecp2*$^{loxP/y}$ mice were indistinguishable from their wild-type littermates (data not shown). Occasionally, we observed seizure behaviors in *Mecp2*$^{T158A/y}$ mice after 5 weeks of age.

Given that *MECP2* is an X-linked gene and that the majority of individuals with RTT are girls with mosaic MeCP2 expression resulting from random X-chromosome inactivation, female *Mecp2*$^{T158A/+}$ mice represent a close genetic match to individuals with RTT. Phenotypic scoring revealed no apparent symptoms in these mice until 17 weeks of age, after which they became progressively and increasingly symptomatic (**Fig. 1d**). A significant increase in body weight also occurred in female *Mecp2*$^{T158A/+}$ mice at the time of symptom presentation ($P < 0.05$; **Supplementary Fig. 2c**), similar to that observed in heterozygous *Mecp2*$^{-/+}$ female mice[12].

An early diagnostic criterion for RTT is a deceleration in head growth, which often leads to microcephaly by the first 2 years of life[3,28]. We observed a significant reduction in the sizes and weights of brains of presymptomatic (postnatal day 30, P30) and postsymptomatic (P90) *Mecp2*$^{T158A/y}$ mice relative to their wild-type littermates ($P < 0.01$; **Fig. 1e**), similar to that observed in *Mecp2*$^{-/y}$ mice[4,5]. The gross brain anatomy of *Mecp2*$^{T158A/y}$ mice, however, was indistinguishable from that of their wild-type littermates (**Supplementary Fig. 2d**). The decreased brain size and weight in *Mecp2*$^{-/y}$ mice are purported to occur, at least in part, through a reduction in neuronal soma size[4,28]. To assess whether soma size is affected in *Mecp2*$^{T158A/y}$ mice, we bred *Mecp2*$^{T158A/y}$ mice to mice expressing GFP under the control of the *Thy1* promoter[29]. Focusing on the hippocampal CA1 region, confocal imaging of GFP-positive pyramidal neurons revealed a significant reduction in soma size in *Mecp2*$^{T158A/y}$ mice compared with wild-type littermates at both P30 and P90 ($P < 0.01$; **Fig. 1f**).

MeCP2 mutation in boys often leads to infantile lethality[3] and male *Mecp2*$^{-/y}$ mice had shortened lifespans[4,5,8]. We found that male *Mecp2*$^{T158A/y}$ mice died prematurely, with 50% dying by 16 weeks of age (**Fig. 1g**), approximately 3–4 weeks later than germline *Mecp2*$^{-/y}$ mice[4,5]. No apparent changes in the survival profiles of female *Mecp2*$^{T158A/+}$ mice were observed before 6 months of age (data not shown). Notably, we did not observe any difference in longevity, body weights or brain weights of *Mecp2*$^{loxP/y}$ mice, supporting the conclusion that these changes are the result of T158A mutation (data not shown). Together, these data suggest that mice carrying the MeCP2 T158A mutation manifest RTT-like phenotypes.

Mecp2$^{T158A/y}$ mice present similar phenotypes as *Mecp2*$^{-/y}$ mice

Given the clinical relevance of the MeCP2 T158A mutation, we sought to carry out a side-by-side comparison of behavioral phenotypes with a well-studied *Mecp2*$^{-/y}$ mouse[5]. In light of the locomotor deficits, aberrant gait and hindlimb clasping observed in these mice (**Supplementary Video 1**), we assessed locomotor activity in a home cage environment with a cohort of age-matched wild-type, *Mecp2*$^{T158A/y}$ and *Mecp2*$^{-/y}$ littermates on the same C57BL/6 background at approximately 9 weeks of age. We found a significant reduction in the locomotor activity of both *Mecp2*$^{T158A/y}$ ($P < 0.01$) and *Mecp2*$^{-/y}$ ($P < 0.001$) mice as compared with wild-type littermates (**Fig. 2a**). However, the reduction in locomotor activity was significantly higher in *Mecp2*$^{-/y}$ mice than in *Mecp2*$^{T158A/y}$ mice ($P < 0.01$; **Fig. 2a**). We also found a significant reduction in the distance traveled by *Mecp2*$^{T158A/y}$ mice at 11 ($P < 0.05$), but not 3, weeks as compared with wild-type littermates using the open field assay (**Supplementary Fig. 3a**). Similarly, locomotor activity was also significantly reduced in female *Mecp2*$^{T158A/+}$ mice at 20 ($P < 0.05$), but not 12, weeks of age (**Supplementary Fig. 3b**), consistent with the age-dependent hypoactivity observed with phenotypic scoring (**Fig. 1c**,**d**).

To examine motor coordination and motor learning in these two mouse models, we performed the accelerating rotarod test. Wild-type mice showed an increase in the latency to fall over the course of four trials per day for 4 d, indicating improvements in motor coordination and learning over time (**Fig. 2b**). However, both *Mecp2*$^{T158A/y}$ and *Mecp2*$^{-/y}$ mice spent significantly less time on the rotarod than wild-type littermates ($P < 0.0001$) and failed to improve over the course of 4 d, suggesting that they had deficits in motor coordination and motor learning (**Fig. 2b**). The latency to fall from the rotarod was moderately, but significantly, decreased in *Mecp2*$^{-/y}$ mice compared with *Mecp2*$^{T158A/y}$ mice ($P < 0.0001$; **Fig. 2b**). We conclude that the MeCP2 T158A mutation impairs motor function similar to that seen in individuals with RTT and to a lesser degree than that seen in *Mecp2* null mice.

Individuals with RTT experience anxiety episodes, particularly in response to distressing events[3]. The role of MeCP2 in anxiety in mice, however, is less clear. *Mecp2* null mice and mice with a 50% reduction in MeCP2 protein expression both show a decreased anxiety phenotype[8–10], whereas those containing an early-truncating mutation show increased anxiety[6]. Using the elevated zero maze procedure, we found that *Mecp2*$^{T158A/y}$ and *Mecp2*$^{-/y}$ mice spent

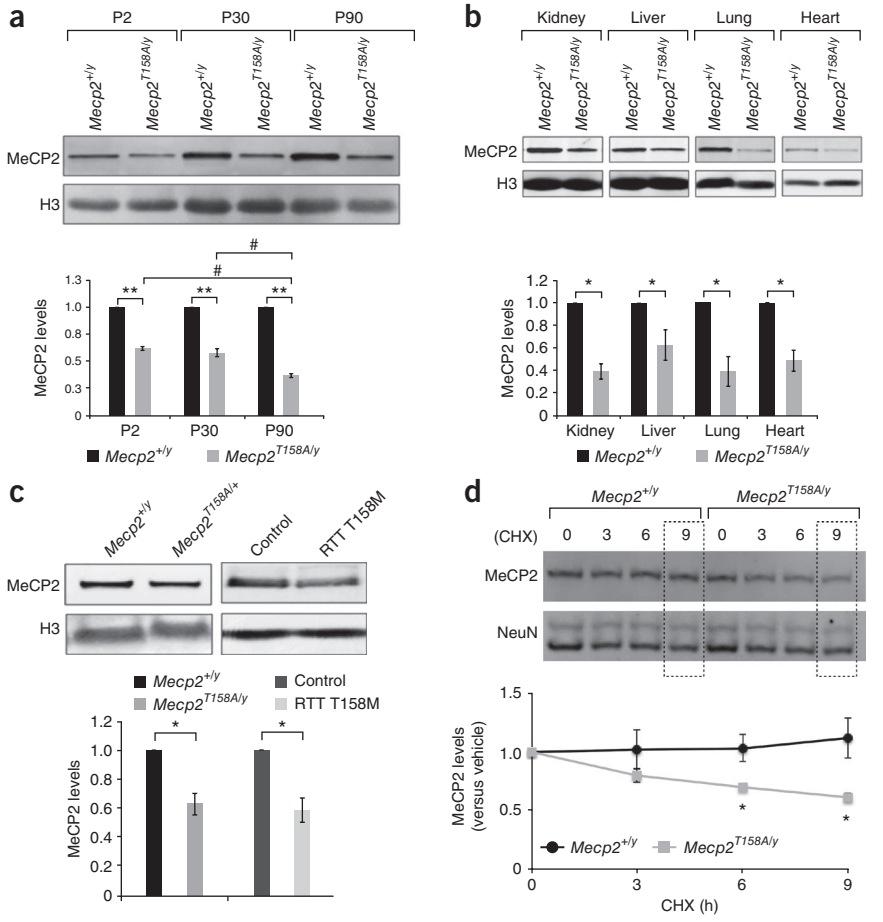

Figure 3 Decreased MeCP2 protein stability in *Mecp2*$^{T158A/y}$ mice. (**a**) MeCP2 protein levels in forebrains of *Mecp2*$^{T158A/y}$ mice at P2, P30 and P90, as compared with *Mecp2*$^{+/y}$ littermates ($n = 3$ for each genotype). Bars represent mean ± s.e.m. $^{**}P < 0.01$, one-sample *t* test with Bonferroni correction; $^{\#}P < 0.05$, one-way ANOVA with Tukey's *post hoc* test. (**b**) MeCP2 protein levels were significantly reduced in kidney, liver, lung and heart tissues of *Mecp2*$^{T158A/y}$ ($n = 3$) compared with *Mecp2*$^{+/y}$ littermates at P90 ($n = 3$). Bars represent mean ± s.e.m. $^{*}P < 0.05$, one-sample *t* test with Bonferroni correction. (**c**) MeCP2 protein levels in female *Mecp2*$^{T158A/+}$ mice ($n = 3$) and *Mecp2*$^{+/y}$ littermates at P90 ($n = 3$). MeCP2 protein levels in fibroblasts derived from a woman with RTT carrying the T158M mutation as compared with fibroblasts derived from an age-matched female control ($n = 3$ separate passages). Bars represent mean ± s.e.m. $^{*}P < 0.05$, one-sample *t* test. (**d**) E16 + 7 d *in vitro* cortical neurons derived from *Mecp2*$^{T158A/y}$ ($n = 3$) and *Mecp2*$^{+/y}$ littermates ($n = 3$) were treated with vehicle (0) or 100 µM CHX for 3, 6 or 9 h. Bars represent mean MeCP2 levels relative to vehicle ± s.e.m. $^{*}P < 0.05$, two-way ANOVA with Bonferroni correction.

significantly less time in the closed arm ($P < 0.01$ and $P < 0.05$, respectively) and significantly more time in the open arm ($P < 0.01$ and $P < 0.05$, respectively) than their wild-type littermates (**Fig. 2c**). This suggests that *Mecp2*$^{T158A/y}$ mice have reduced anxiety, similar to what we observed in *Mecp2*$^{-/y}$ mice and mice with decreased MeCP2 protein expression.

Because RTT is the primary cause of intellectual disability in females, we examined whether MeCP2 mutant mice have learning and memory deficits using contextual and cued fear-conditioning procedures. Mice were trained to associate a context (testing box) and a cue (auditory tone) with a co-terminating foot shock. Mice typically freeze in response to the shock. We found no differences in freezing behaviors in wild-type and *Mecp2*$^{T158A/y}$ littermates before or immediately following shocks, suggesting that there were no differences in pain sensitivity. However, *Mecp2*$^{-/y}$ mice exhibited significantly increased freezing even before the shock ($P < 0.01$; **Supplementary Fig. 3c**). This is likely a result of their decreased locomotor activity and akinesia, thus confounding interpretation of the fear-conditioning test. These mice were therefore excluded from this study. *Mecp2*$^{T158A/y}$ mice showed significantly less context-dependent ($P < 0.05$) and cue-dependent ($P < 0.001$) freezing than their wild-type littermates at 24 h after training, suggesting that they have deficits in learning and memory (**Fig. 2d**).

Together, these findings indicate that *Mecp2*$^{T158A/y}$ mice have phenotypes similar to those observed in *Mecp2*$^{-/y}$ mice, but to a lesser extent overall. We therefore infer that T158A is a partial loss-of-function mutation.

Decreased MeCP2 protein stability in *Mecp2*$^{T158A/y}$ mice

Alterations in MeCP2 protein levels, such as a 50% reduction or a twofold increase, leads to the progressive development of neurological deficits in mice, albeit at much later time points than those observed in *Mecp2* null mice[7,9,10]. We therefore examined whether the T158A mutation alters the expression of MeCP2 protein during development. Quantitative western blotting on whole-cell lysates from the brains of male *Mecp2*$^{T158A/y}$ mice revealed that MeCP2 protein expression was significantly decreased at P2, P30 and P90 compared with their wild-type littermates ($P < 0.01$; **Fig. 3a**). The downregulation of MeCP2 expression was significantly higher at P90 ($P < 0.05$), when *Mecp2*$^{T158A/y}$ mice presented overt RTT-like phenotypes, than at either P2 or P30, when symptoms were not present (**Fig. 1c**). Notably, MeCP2 protein levels were not affected in *Mecp2*$^{loxP/y}$ mice, indicating that the downregulation of MeCP2 is a result of the presence of the T158A mutation rather than of genomic modification (**Fig. 1b**). These changes in MeCP2 expression are likely to be independent of gene transcription, as quantitative real-time reverse-transcription PCR (RT-PCR) revealed no differences in the level of *Mecp2* mRNA expression between *Mecp2*$^{T158A/y}$ and wild-type mice at P0, P30 or P90 (**Supplementary Fig. 4**). Despite RTT being primarily a neurological disorder[3], MeCP2 is ubiquitously expressed in all mammalian tissues[30]. Indeed, we found that MeCP2 protein levels were decreased to a similar extent in kidney, liver, lung and heart in *Mecp2*$^{T158A/y}$ mice (**Fig. 3b**).

MeCP2 protein levels were also significantly decreased in the brains of female *Mecp2*$^{T158A/+}$ mice as compared with their wild-type littermates ($P < 0.05$; **Fig. 3c**). The magnitude of MeCP2 downregulation in females was less than that observed in male *Mecp2*$^{T158A/y}$ mice and was likely a result of the mosaic expression of MeCP2 T158A in heterozygous *Mecp2*$^{T158A/+}$ mice. To investigate whether mutation at T158 disrupts MeCP2 protein expression in individuals with RTT, we obtained fibroblast cultures derived from an affected female with the T158M mutation and an age-matched female control. We found that

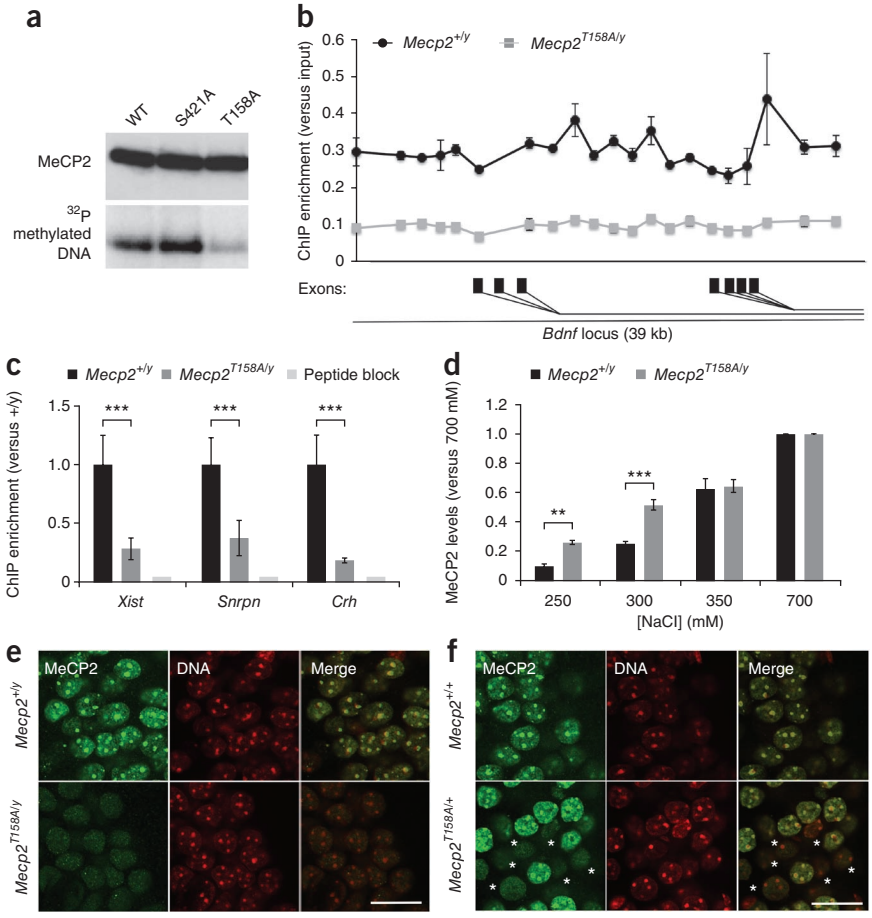

Figure 4 Reduced MeCP2 binding to methylated DNA in *Mecp2*$^{T158A/y}$ mice. (**a**) MeCP2 binding to methylated DNA (methylated oligonucleotides spanning the –148 CpG site of Bdnf promoter IV) was reduced by the T158A mutation relative to wild-type (WT) and S421A MeCP2 in a Southwestern assay. (**b**) MeCP2 binding across 39 kb of the promoter region of the *Bdnf* locus in brains obtained from *Mecp2*$^{T158A/y}$ mice and *Mecp2*$^{+/y}$ littermates ($n = 3$, two-way ANOVA, $F_{1,84} = 639.1$, $P < 0.0001$). Symbols represent mean ± s.e.m. Alternative *Bdnf* exons are indicated with black rectangles. (**c**) MeCP2 binding to the *Xist*, *Snrpn* and *Crh* loci in *Mecp2*$^{T158A/y}$ mice ($n = 3$) as compared with *Mecp2*$^{+/y}$ littermates ($n = 3$). Bars represent mean ± s.e.m. ***$P < 0.001$, two-tailed *t* test with Bonferroni correction. (**d**) Salt extraction of wild-type MeCP2 and MeCP2 T158A with increasing concentrations of NaCl ($n = 3$). Bars represent mean ± s.e.m. normalized to MeCP2 levels extracted with 700 mM NaCl. **$P < 0.01$ and ***$P < 0.001$, two-way ANOVA with Bonferroni correction. (**e**) MeCP2 co-localization with heterochromatin-dense foci in male *Mecp2*$^{+/y}$, but not *Mecp2*$^{T158A/y}$, mice at P90. The representative images of neuronal nuclei that are shown are single confocal planes at 100× magnification. Scale bar corresponds to 20 μm. (**f**) MeCP2 staining in nuclei obtained from female *Mecp2*$^{T158A/+}$ mice. Nuclei showing diffuse MeCP2 staining are marked with an asterisk. Scale bar corresponds to 20 μm.

MeCP2 expression was also significantly downregulated by about 40% in cells with the MeCP2 T158M mutation compared with control cells ($P < 0.05$; **Fig. 3c**). These data indicate that T158 mutation, to either alanine or methionine, triggers the downregulation of MeCP2 protein expression in both humans and mice, indicating that the reduction in MeCP2 protein expression may be a contributing factor to RTT.

To investigate whether the reductions in MeCP2 protein levels are a consequence of decreased protein stability, we cultured embryonic day 16 (E16) cortical neurons isolated from wild-type and *Mecp2*$^{T158A/y}$ mice and inhibited new protein translation using cycloheximide (CHX). The stability of existing MeCP2 protein was assessed at 0, 3, 6 and 9 h following CHX treatment. We found that MeCP2 protein levels in wild-type neurons remained relatively constant over the course of the 9-h CHX treatment as compared with vehicle-treated cultures (**Fig. 3d**). In contrast, MeCP2 T158A protein levels were significantly reduced following 6- and 9-h CHX treatments ($P < 0.05$; **Fig. 3d**), suggesting that the T158A mutation decreased MeCP2 protein levels by increasing its rate of degradation. We did not observe destabilization of other proteins, such as NeuN in T158A mice (**Fig. 3d**). Thus, the *Mecp2*$^{T158A/y}$ mice have revealed a previously unknown function of T158 in the stabilization of MeCP2 protein *in vivo*. The reduction in MeCP2 protein stability mediated by the T158A mutation may contribute, at least in part, to the etiology of RTT.

T158A mutation disrupts MeCP2 binding to methylated DNA

Located at the 3′ end of the MBD, T158 is believed to be important for stabilizing the tertiary structure of MBD and is critical for the binding of MeCP2 to methylated DNA[14]. We recapitulated these *in vitro* observations using a Southwestern assay (**Fig. 4a**). To examine the role of T158 in the regulation of MeCP2 binding to methylated DNA *in vivo*, we isolated nuclei from the brains of wild-type and *Mecp2*$^{T158A/y}$ mice and performed chromatin immunoprecipitation (ChIP) assays against several known MeCP2-binding loci. MeCP2 has been shown to bind across a 39-kb promoter region of the *Bdnf* locus tracking methyl-CpG sites[31]. Consistent with this, we found a similar MeCP2-binding pattern in brains from P60 wild-type mice (**Fig. 4b**). MeCP2 ChIP over the same region in *Mecp2*$^{T158A/y}$ brains, however, revealed a 70–75% reduction in MeCP2 binding across the entire locus (**Fig. 4b**), suggesting that the T158A mutation decreases MeCP2 binding at methylated DNA. To validate this finding, we also analyzed the binding of MeCP2 to the *Xist*, *Snrpn* and *Crh* loci, which are known MeCP2-binding targets[31,32], and found that the binding of MeCP2 at these loci was significantly reduced by approximately 70% in *Mecp2*$^{T158A/y}$ brains ($P < 0.001$; **Fig. 4c**). Thus, the reduction of MeCP2 binding at the *Bdnf*, *Xist*, *Snrpn* and *Crh* loci likely reflects a decreased binding of MeCP2 T158A to methylated DNA together with reduced MeCP2 protein expression.

We reasoned that if MeCP2 T158A has a reduced affinity for methylated DNA *in vivo*, wild-type or MeCP2 T158A protein would be extracted differently from nuclei under the same salt conditions. To biochemically assay the reduced affinity of MeCP2 T158A to methylated DNA, we isolated neuronal nuclei from either wild-type or *Mecp2*$^{T158A/y}$ mouse brains and treated them with increasing concentrations of NaCl to extract proteins into the supernatant. Quantitative western blot analysis revealed that MeCP2 T158A protein was extracted more readily than wild-type protein under low-salt conditions of 250 mM and 300 mM NaCl (**Fig. 4d**). When the salt

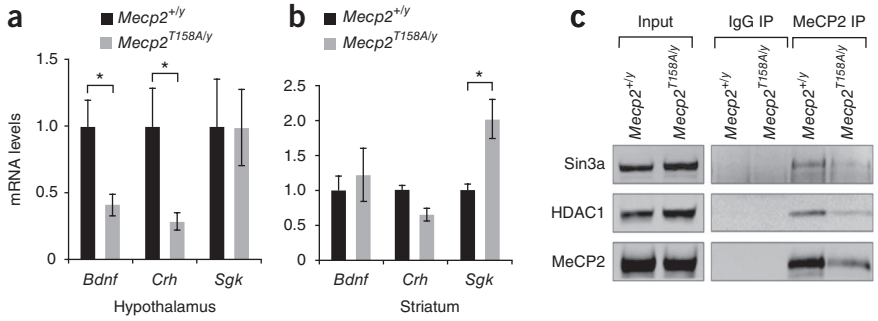

Figure 5 Disruption of MeCP2 methyl-DNA binding leads to deregulation of gene expression. (**a**) *Bdnf*, *Crh* and *Sgk* mRNA expression in the hypothalamus of $Mecp2^{T158A/y}$ mice as compared with $Mecp2^{+/y}$ littermates ($n = 4$). Bars represent mean ± s.e.m. $^*P < 0.05$, two-tailed *t* test with Bonferroni correction. (**b**) *Bdnf*, *Crh* and *Sgk* mRNA expression in the striatum of $Mecp2^{T158A/y}$ mice and $Mecp2^{+/y}$ littermates ($n = 4$). Bars represent mean ± s.e.m. $^*P < 0.05$, two-tailed *t* test with Bonferroni correction. (**c**) The T158A mutation did not impair the association of MeCP2 with HDAC1 or Sin3a. MeCP2 immunoprecipitation (IP) from brain nuclear extracts prepared from $Mecp2^{T158A/y}$ and $Mecp2^{+/y}$ littermates are probed with indicated antibodies.

concentration was raised to above 350 mM, both wild-type and T158A protein were extracted to a similar degree. Thus, the T158A mutation appears to decrease the affinity of MeCP2 for DNA.

MeCP2 predominantly associates with heterochromatic foci in mouse cell nuclei in an MBD- and DNA methylation–dependent manner, resulting in a characteristic punctate pattern of nuclear staining[33]. Indeed, MeCP2 immunoreactivity was observed throughout the nucleus, with particularly high enrichment at heterochromatin-dense foci in nuclei from P90 wild-type neurons (**Fig. 4e**). In contrast, in nuclei from P90 $Mecp2^{T158A/y}$ neurons, MeCP2 was markedly diffuse with a clear absence of co-localization with DNA, indicating that the binding of MeCP2 to methylated DNA was disrupted (**Fig. 4e**). It is unlikely that this difference is a result of changes in heterochromatin formation, as no overt differences were seen in DNA staining in $Mecp2^{T158A/y}$ mice. We observed similar immunoreactivity patterns in P30 $Mecp2^{T158A/y}$ mice before symptom presentation (data not shown). Furthermore, MeCP2 immunoreactivity in female $Mecp2^{T158A/+}$ mice revealed a mosaic expression of MeCP2, with approximately 50% of nuclei showing MeCP2 immunoreactivity at heterochromatin-dense foci and the remaining exhibiting diffuse immunoreactivity (**Fig. 4f**), as would be expected as a result of random X-chromosome inactivation. Notably, the intensity of MeCP2 immunoreactivity was decreased in $Mecp2^{T158A/y}$ neurons compared with wild-type neurons, consistent with a reduction of MeCP2 T158A protein expression. Together, these findings suggest that the T158A mutation impairs the binding of MeCP2 to methylated DNA *in vivo* and contributes, at least in part, to the etiology of RTT.

Disruption of transcription by MeCP2 T158A

Transcriptional profiling of RNA isolated from the hypothalamus or cerebellum of $Mecp2^{-/y}$ mice revealed changes in the expression of hundreds of genes[32]. We analyzed the expression of a few representative targets, such as *Bdnf*, *Crh* and *Sgk*, using quantitative RT-PCR and found that both *Bdnf* and *Crh* transcription were significantly reduced in the hypothalamus, but not striatum, of $Mecp2^{T158A/y}$ mice ($P < 0.05$; **Fig. 5a**,**b**), whereas *Sgk*, a gene that is upregulated in $Mecp2^{-/y}$ mice[34], was elevated in the striatum, but not in the hypothalamus, of $Mecp2^{T158A/y}$ mice (**Fig. 5a**,**b**). These data support the idea that gene transcription is similarly disrupted in $Mecp2^{T158A/y}$ and $Mecp2^{-/y}$ mice in a tissue- and/or cell type–specific manner.

MeCP2 has been shown to regulate gene transcription through its interaction with histone deacetylases (HDACs) 1 and 2 and the co-repressor Sin3a[35,36]. It is conceivable that the T158A mutation may disrupt the ability of MeCP2 to associate with these proteins through alterations in the conformation of MeCP2 and thus disrupt downstream gene regulation. We therefore performed co-immunoprecipitation experiments using an antibody to MeCP2 in nuclear extracts prepared from wild-type and $Mecp2^{T158A/y}$ brains. Consistent with previous findings, wild-type MeCP2 interacted with HDAC1 and Sin3a (**Fig. 5c**). MeCP2 T158A also associated with HDAC1 and Sin3A, albeit at a reduced level, consistent with the reduction in MeCP2 T158A protein expression (**Fig. 5c**). These data support the idea that MeCP2 T158A protein retains the ability to interact with the co-repressor proteins. Thus, we conclude that the T158A mutation leads to a deregulation of gene expression through reduced DNA binding and MeCP2 protein stability.

Age-dependent alterations in EEG and ERP recordings

The manifestations of symptoms in individuals with RTT and *Mecp2* null mice are thought to occur in part because of alterations in neural network activity. Given that RTT symptoms appear at certain developmental time points, we sought to investigate the neural mechanisms underlying age-dependent exhibition of phenotypes in $Mecp2^{T158A/y}$ mice. Thus, we performed EEG recordings in wild-type and $Mecp2^{T158A/y}$ mice at two developmental time periods, P30 and P90; that is, before and subsequent to the establishment of RTT-like symptoms. EEG recordings in awake, freely mobile mice revealed a significant increase in the power of high-gamma frequency (γ_{high}, 70–140 Hz) oscillations in $Mecp2^{T158A/y}$ mice at P90 compared with wild-type littermates ($P < 0.001$; **Fig. 6a**,**b**). A similar increase in γ_{high} power was also observed in symptomatic $Mecp2^{-/y}$ mice (**Supplementary Fig. 5a**,**b**). γ_{high} activity is known to be associated with epilepsy in the EEG before and during seizure[37] and may reflect an overall hyperexcitability in the brains of $Mecp2^{T158A/y}$ and $Mecp2^{-/y}$ mice[22]. However, we did not observe an increase in γ_{high} power in pre-symptomatic $Mecp2^{T158A/y}$ mice at P30 (**Supplementary Fig. 6a**,**b**), suggesting that MeCP2 dysfunction induces hyperexcitability in the brain in an age-dependent manner.

In addition to measuring electrical activity during passive processes, it is also possible to measure those that occur during the performance of a cognitive, sensory or motor task. The manifestation of these brain activities is recorded as a series of amplitude deflections in the EEG as a function of time and is referred to as an ERP. ERPs are small compared with the background EEG, but can be resolved by averaging single trial epochs. They are characterized as voltage deflections defined by latency and polarity, where the amplitude and latency of the polarity peaks are believed to reflect the strength and timing of the cognitive processes related to the event. Notably, individuals with RTT, as well as those with schizophrenia and autism, show alterations in both the amplitudes and latencies of ERPs[19–21,24,25].

To examine ERP responses in $Mecp2^{T158A/y}$ mice, we performed EEG recordings following the presentation of a series of white noise clicks. We chose to perform auditory-evoked ERP assessments because they can be performed on freely mobile mice and are not

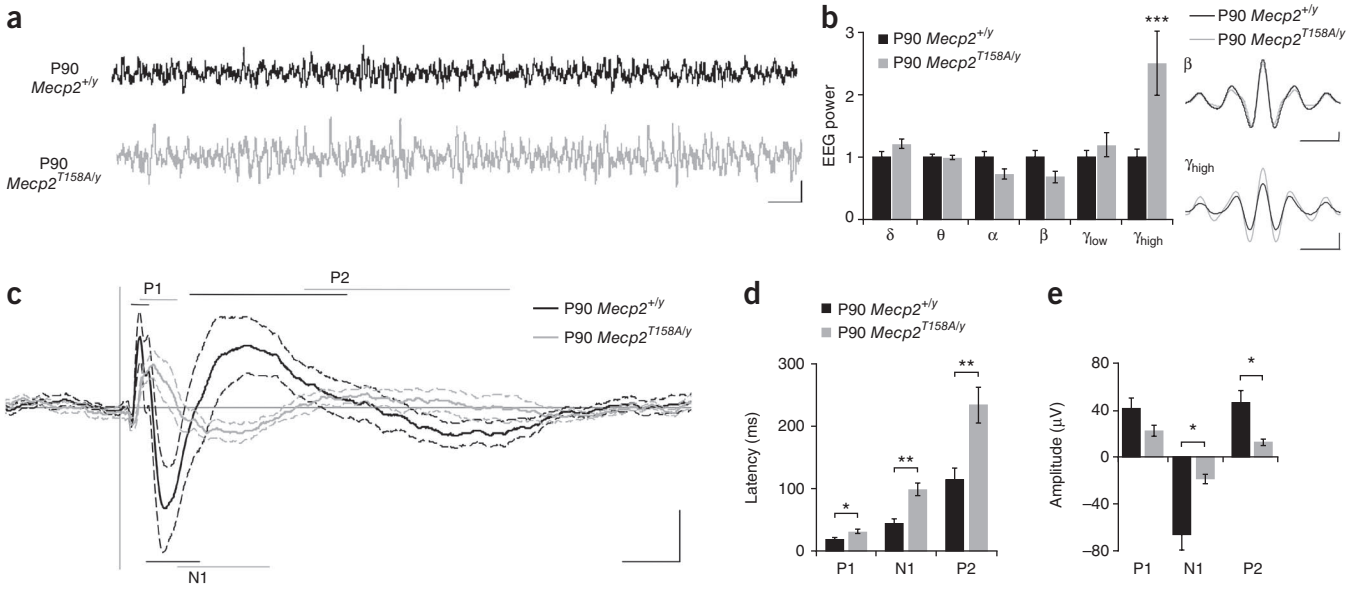

Figure 6 EEG and ERP recordings in *Mecp2*$^{T158A/y}$ mice. (**a**) Representative EEG traces from awake, freely mobile mice. Scale bar corresponds to 1 s (horizontal) and 200 μA (vertical). (**b**) Basal EEG power measurements in P90 *Mecp2*$^{T158A/y}$ mice ($n = 7$) compared with *Mecp2*$^{+/y}$ littermates ($n = 8$). Frequency bands are represented as follows: δ (2–4 Hz), θ (4–8 Hz), α (8–12 Hz), β (12–30 Hz), γ_{low} (30–50 Hz) and γ_{high} (70–140 Hz). Insets show β and γ_{high} mean amplitudes across EEG recordings. Scale bars represent one oscillation cycle (horizontal) and 20 μA (vertical). Bars represent mean ± s.e.m. ***$P < 0.001$, two-tailed *t* test with Bonferroni correction. (**c**) Grand average ERP traces following presentation of 85-dB white-noise clicks with 4-s interstimulus intervals. Traces represent mean amplitude (solid line) ± s.e.m. (dashed lines). The characteristic polarity peaks P1, N1 and P2 are highlighted with straight lines with the length indicating latency range. Scale bar corresponds to 50 ms (horizontal) and 20 μA (on vertical). (**d**,**e**) Latencies (**d**) and amplitudes (**e**) of ERP peaks. Bars represent mean ± s.e.m. *$P < 0.05$ and **$P < 0.01$, two-tailed *t* test with Bonferroni correction.

confounded by the motor or attentional deficits associated with MeCP2 dysfunction. The ERP was extracted by averaging the EEG traces over single trial epochs. ERPs in wild-type and *Mecp2*$^{T158A/y}$ mice showed a stereotypical initial positive peak (P1), followed by a negative peak (N1) and a subsequent second positive peak (P2) (**Fig. 6c**). Notably, we found significant increases in the latency of P1 ($P < 0.05$), N1 and P2 peaks ($P < 0.01$) and significant reductions in the amplitudes of the N1 and P2 peaks ($P < 0.05$) in symptomatic P90 *Mecp2*$^{T158A/y}$ mice compared with wild-type littermates (**Fig. 6c–e**). Similar alterations in ERP amplitudes and latencies were observed in *Mecp2*$^{-/y}$ mice (**Supplementary Fig. 5c–e**). However, we observed no effect on ERPs in *Mecp2*$^{T158A/y}$ mice at P30, before the establishment of RTT-like symptoms (**Supplementary Fig. 6c–e**). Notably, we found no differences in hearing sensitivities between *Mecp2*$^{T158A/y}$ mice or *Mecp2*$^{-/y}$ mice and their wild-type littermates as measured by auditory brain stem responses, suggesting that these disruptions in ERP are a result of alterations in cortical processing of sensory input (**Supplementary Fig. 7**). These data suggest that the neural networks underlying information processing are disrupted by MeCP2 dysfunction in an age-dependent manner, corresponding to the behavioral onset of symptoms.

Progressive alterations in event-related power and PLF

One limitation of time-amplitude analysis of ERPs is that oscillatory information that is not time-locked to the stimulus is lost through signal averaging. Using time-frequency analysis, it is possible to analyze changes in oscillatory activity as a function of time and thus gain additional insight into the underlying brain activity and circuitry. Oscillatory responses during the performance of tasks are characterized by the average power and phase locking across trials[38]. The degree of event-related power and phase locking at different frequencies may reflect the strength and connectivity of local (at high frequencies) and long-range (at low frequencies) neuronal circuits[39].

Thus, we next performed time-frequency analysis on EEG recordings used to determine auditory-evoked ERPs. We found that wild-type mice at P90 showed a significant depression in the mean power of oscillations in the low-frequency delta (δ, 2–4 Hz), theta (θ, 4–8 Hz) and alpha (α, 8–12 Hz) ranges on auditory stimulation (**Fig. 7a**,**b**). The mean event-related power of high-frequency beta (β, 12–30 Hz), low gamma (γ_{low}, 30–50 Hz) and γ_{high} (70–140 Hz) increased following the auditory stimulus and was followed by a sustained depression in power (**Fig. 7a**,**b**). Notably, these changes were sustained for a number of oscillation cycles at all frequencies and outlasted the transient ERP response, reflecting an effect in both evoked and ongoing oscillatory processes (**Fig. 7a**,**b**). Overlaying the ERP with band-pass EEG traces at each frequency range also revealed the oscillatory information in the transient ERP response (**Supplementary Fig. 8**). *Mecp2*$^{T158A/y}$ mice, however, exhibited significantly attenuated event-related power in both low- and high-frequency oscillations at P90 ($P < 0.001$), when RTT-like symptoms were overt (**Fig. 7a**,**b** and **Supplementary Fig. 9a**). Similarly, highly symptomatic *Mecp2*$^{-/y}$ mice showed significantly reduced event-related power following auditory stimulation at all frequencies ($P < 0.001$; **Supplementary Figs. 9b** and **10a**,**b**). Notably, we also found a small, but significant, reduction in event-related power in low-frequency δ, θ and α in P30 *Mecp2*$^{T158A/y}$ mice prior to symptom onset compared with wild-type littermates ($P < 0.05$), in contrast with that observed using time-amplitude analysis (**Supplementary Figs. 9c** and **11a**,**b**). These data suggest that the underlying deficits in neural activity occur before the establishment of behavioral symptoms, consistent with *in vitro* electrophysiological studies showing reduced cortical excitability in *Mecp2*$^{-/y}$ mice even at 2–3 weeks of age[15].

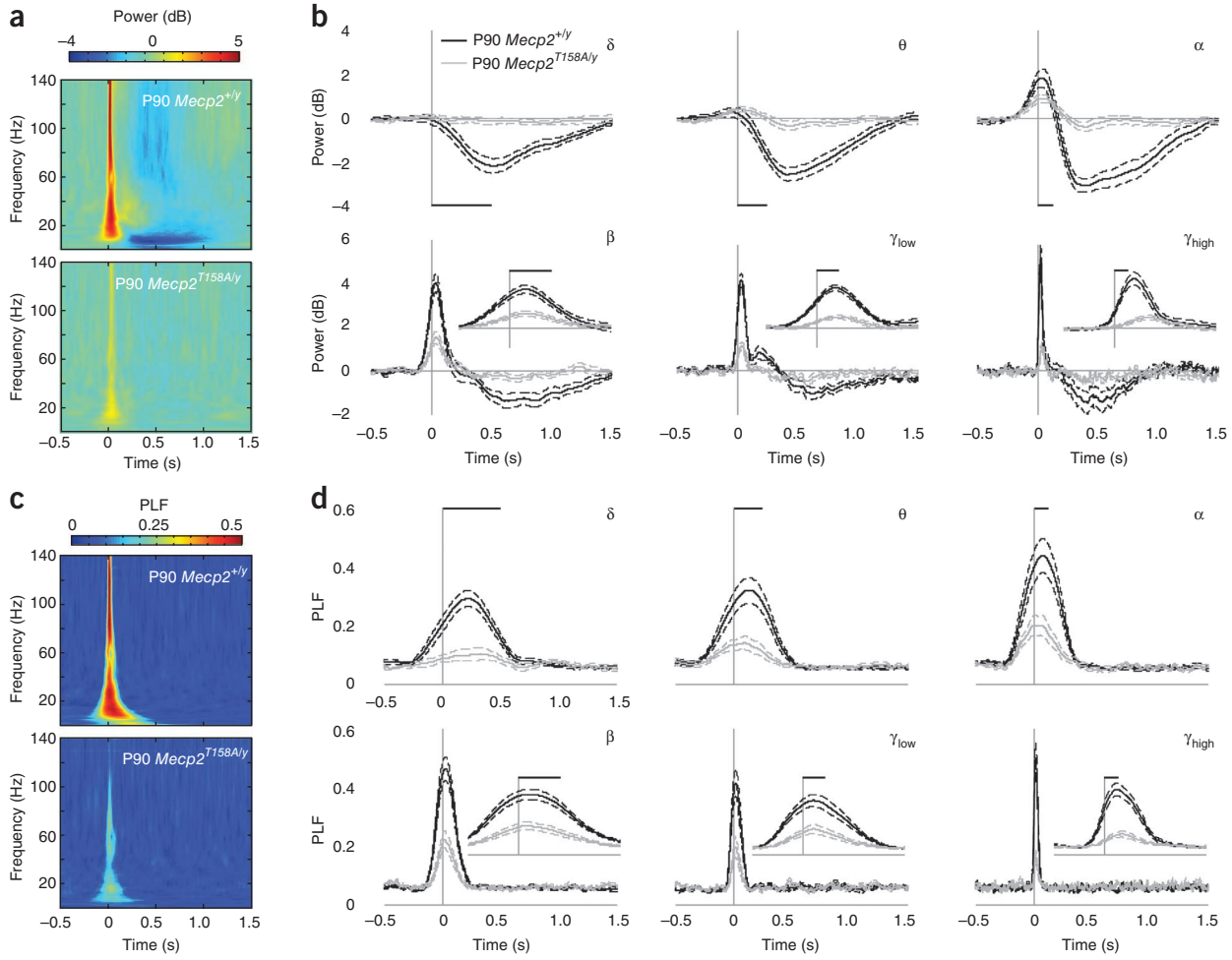

Figure 7 Decreased event-related power and PLF in *Mecp2*$^{T158A/y}$ mice. (**a**) Time-frequency plots showing changes in event-related power in response to 85-dB auditory stimulation in P90 *Mecp2*$^{T158A/y}$ mice and *Mecp2*$^{+/y}$ littermates. Time is plotted on the abscissa (where $t = 0$ at sound presentation) and frequency on the ordinate. Color represents mean power with warmer colors corresponding to an increased power and cooler colors representing decreased power compared to prestimulus baseline. (**b**) Changes in event-related mean power averaged across δ (2–4 Hz), θ (4–8 Hz), α (8–12 Hz), β (12–30 Hz), γ_{low} (30–50 Hz), and γ_{high} (70–140 Hz) frequencies. Scale bars represent the length of a single oscillation cycle of the lowest frequency in the range. Insets showed power traces on expanded timescale denoted by length of single oscillation cycle. Traces represent mean power ± s.e.m. (**c**) Time-frequency plots showing changes in event-related PLF in response to 85-dB auditory stimulation. Color represents PLF with warmer colors corresponding to a higher PLF or lower circular variance in EEG phase across trials. (**d**) Changes in event-related PLF averaged across frequencies as described above. Scale bars represent the length of a single oscillation cycle and insets show traces on expanded timescale. Traces represent mean PLF ± s.e.m.

Time-frequency analysis also allows for the calculation of oscillation phase locking across trials. The phase-locking factor (PLF) quantifies the trial-to-trial reliability of oscillation phase, with a high PLF corresponding to a low circular variance in oscillation phase as a function of time between trials. A high PLF is thought to reflect the reliability and sensitivity of communications between circuits in the brain[40]. We found that wild-type mice at P90 showed increases in PLF at all frequencies in response to the presentation of auditory stimuli (**Fig. 7c**,**d**). The increase in PLF in *Mecp2*$^{T158A/y}$ mice at P90, however, was significantly reduced compared with that of wild-type mice ($P < 0.01$ for θ, α and γ_{low}, $P < 0.001$ for δ, β and γ_{high}; **Fig. 7c**,**d** and **Supplementary Fig. 9d**). A significant reduction in event-related PLF in *Mecp2*$^{-/y}$ mice was also observed ($P < 0.05$ for γ_{low}, $P < 0.01$ for θ, α and β, $P < 0.001$ for δ and γ_{high}), consistent with the expression of RTT-like phenotypes in both groups of mice (**Supplementary Figs. 9e** and **10c**,**d**). We detected significant attenuation in PLF in presymptomatic P30 *Mecp2*$^{T158A/y}$ mice, but only at δ and γ_{high} frequencies ($P < 0.05$; **Supplementary Figs. 9f** and **11c**,**d**). Notably, the fact that we did not observe changes in ERP amplitudes at P30 in *Mecp2*$^{T158A/y}$ mice (**Supplementary Figs. 6** and **12**) suggests that time-frequency analysis of event-related power and PLF represents a sensitive approach for probing neural function *in vivo*.

When comparing the event-related neuronal responses in wild-type mice at two developmental stages, we found that event-related power at all frequencies and PLF at high frequencies were significantly higher in P90 mice than in P30 mice ($P < 0.05$ for β and γ_{low}, $P < 0.01$ for γ_{high}; **Fig. 8a**,**b**). This likely reflects the development and maturation of the underlying neuronal circuitry. In contrast, *Mecp2*$^{T158A/y}$ mice did not show a developmental increase in either event-related power (**Fig. 8c**) or phase locking (**Fig. 8d**) from P30 to P90, suggesting an impairment in age-dependent neural network maturation. These age-dependent differences were observed using time-frequency analysis, but not using time-amplitude analysis (**Fig. 8** and **Supplementary Fig. 12**). Together, these data suggest that MeCP2 is important for the regulation of event-related neuronal responses and is required for the maturation and restructuring of neural networks. The disruptions in

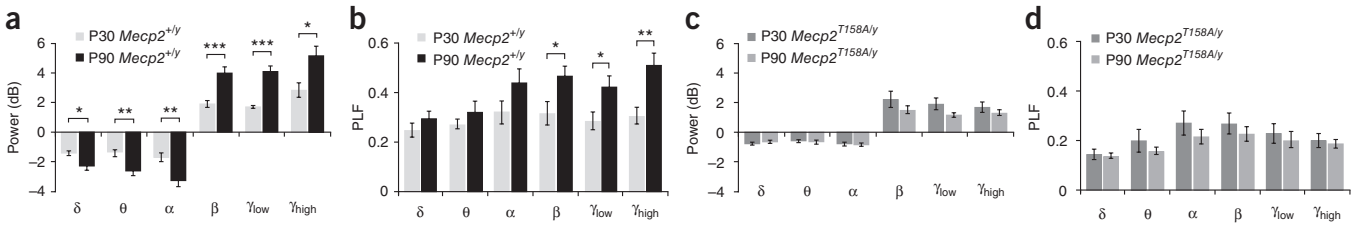

Figure 8 Age-dependent increase in event-related power and PLF is absent in *Mecp2*$^{T158A/y}$ mice. (**a**) Event-related power changes in *Mecp2*$^{+/y}$ mice at P30 and P90. (**b**) Event-related phase-locking factor (PLF) changes in *Mecp2*$^{+/y}$mice at P30 and P90. (**c**) Event-related power changes in *Mecp2*$^{T158A/y}$ mice at P30 and P90. (**d**) Event-related PLF changes in *Mecp2*$^{T158A/y}$ mice at P30 and P90. Bars represent mean ± s.e.m. $^{*}P < 0.05$, $^{**}P < 0.01$ and $^{***}P < 0.001$, two-tailed *t* test with Bonferroni correction.

event-related power and PLF may therefore contribute to the deficits in behavioral and cognitive functions that are observed in RTT. We propose that ERP studies may serve as a sensitive biomarker for the evaluation of treatments in individuals with RTT.

DISCUSSION

Mutation of threonine 158 to methionine or, in rare cases, alanine in MeCP2 represents one of the most common mutations observed in individuals with RTT[2]. Previous *in vitro* experiments have established a critical role for this residue in the binding of MeCP2 to methylated DNA. To address the causal role of the T158A mutation in the pathogenesis of RTT and the role of methyl-DNA binding in the proper functions of MeCP2, we developed and characterized *Mecp2*$^{T158A/y}$ mice. We found that *Mecp2*$^{T158A/y}$ mice developed normally for the first 4–5 weeks of life, after which they presented RTT-like symptoms, including decreased motor performance, altered anxiety, aberrant gait, hindlimb clasping, breathing abnormalities, and impaired learning and memory. The similarity in the identity and severity of symptoms with those observed in *Mecp2* null mice indicates that the T158A mutation is a partial loss-of-function mutation.

The development of this mouse line allowed us to investigate the biochemical consequences of the T158A mutation *in vivo*. Consistent with previous *in vitro* studies, we found that the T158A mutation led to a reduction in the affinity of MeCP2 for methylated DNA *in vivo*. Notably, we also observed that the T158A mutation concomitantly decreased MeCP2 protein expression *in vivo*. Consistent with these data, we found that fibroblasts obtained from a woman with RTT carrying the MeCP2 T158M mutation expressed decreased levels of MeCP2 protein. These findings reveal two consequences of T158 mutation: impaired MeCP2 binding to DNA and decreased MeCP2 protein stability.

Previous studies have shown that MeCP2 protein levels must be tightly regulated to ensure its proper function. A 50% reduction in MeCP2 protein expression leads to progressive neurological symptoms[9,10], although symptoms appear later and do not fully recapitulate the RTT-like symptoms seen in *Mecp2* null mice. Thus, the destabilization of MeCP2 protein alone, as observed in our *Mecp2*$^{T158A/y}$ mice, may not be sufficient to cause the RTT-like symptoms. We propose that the combined reduction in MeCP2 protein levels and the decreased binding to methylated DNA contribute to the loss-of-function phenotype in *Mecp2*$^{T158A/y}$ mice. The development of knockin mice carrying other mutations that disrupt DNA binding will provide further insights into this hypothesis. Given that the reintroduction of MeCP2 protein into *Mecp2* null mice is sufficient to rescue RTT-like phenotypes[12], we suggest a dual approach to restore MeCP2 function in individuals carrying MeCP2 T158 mutations: increasing MeCP2 affinity for methylated DNA and enhancing MeCP2 protein stability. Indeed, the feasibility of increasing affinity for DNA has been shown for other DNA-binding proteins such as p53 (ref. 41). It is conceivable that increasing MeCP2 affinity for methylated DNA may help to stabilize MeCP2 protein expression. Utilizing one or both of these approaches may lead to the amelioration of RTT-like phenotypes. Our findings also suggest that different therapeutic strategies should be considered for treating individuals with different MeCP2 mutations.

Given their neurological origin, many of the symptoms associated with RTT have been hypothesized to result from imbalanced neural networks[3]. Evidence to support this arises from observed alterations in synaptic connectivity and plasticity[12,15–17,42] and hyperexcitability in the EEGs[22,23] of *Mecp2*$^{-/y}$ mice. Furthermore, ERP analysis in women with RTT suggests that alterations occur in the sensory processing of information[24,25]. Given the delayed onset of symptoms in individuals with RTT, *Mecp2*$^{T158A/y}$ mice and *Mecp2*$^{-/y}$ mice, we sought to examine whether neurophysiological responses, as measured by EEG, are altered during development in *Mecp2*$^{T158A/y}$ mice. Indeed, we found that the power of γ_{high} EEG signals was substantially increased in *Mecp2*$^{T158A/y}$ mice when these mice exhibited RTT-like symptoms, suggesting hyperexcitability in the brain. Furthermore, assessment of auditory-evoked ERPs revealed a substantial reduction in the amplitude and increased latency of ERPs in *Mecp2*$^{T158A/y}$ and *Mecp2*$^{-/y}$ mice, suggesting that there are deficits in information processing in the brain similar to those observed in women with RTT[24,25], in autism[20,21] and in other disorders including schizophrenia[18]. Further studies are needed to address the neuronal mechanisms that underlie these deficits in ERP response.

Our data suggest that disturbances in event-related power and phase locking also occur in MeCP2 mouse models and may be involved in the etiology of RTT. In humans and animal models, changes in the power and phase locking of neuronal responses coordinate neuronal activity across different brain regions. These changes are involved in the development and efficacy of motor, perceptual and memory tasks, and deficits in neuronal oscillations are consistently observed in neurological disorders in which these functions are impaired[18,43]. Our finding that both low- and high-frequency event-related oscillations were disrupted led us to hypothesize that deficits in local and long-distance neuronal circuitry occur following MeCP2 dysfunction. The neurophysiological mechanisms that lead to disturbances in these oscillations are not known, but may involve the reduced neuronal connectivity that leads to a redistribution of neuronal activity away from excitation and toward inhibition as observed in *Mecp2*$^{-/y}$ mice[15–17]. Furthermore, given the importance of event-related neuronal responses in the development of the nervous system[44], their disruption before symptom presentation may augment the deficits in neuronal activity caused by MeCP2 dysfunction. Indeed, *Mecp2*$^{T158A/y}$ mice did not exhibit developmental increases in event-related power or phase locking suggestive of stagnation in the developmental of neuronal circuits. Moreover, our finding that event-related changes in power and phase locking occurred in *Mecp2*$^{T158A/y}$ mice with no behavioral

symptoms suggests that disruptions in neuronal networks may precede the behavioral RTT-like phenotypes. The identification of the mechanisms that lead to these disturbances will provide valuable insights into the pathogenesis of RTT and the neuronal networks underlying the manifestation of behavioral phenotypes in RTT.

In summary, using *Mecp2*$^{T158A/y}$ mice, we uncovered a previously unknown role for T158 in the pathogenesis of RTT and revealed an alternative strategy for restoring MeCP2 function. These mice provide an *in vivo* animal model for assessing therapeutic efficacy in preclinical trials. Moreover, given that ERP studies can be readily performed in humans, assessment of ERP and the changes in oscillation and phase locking may serve as a valuable biomarker for evaluating RTT phenotypes.

METHODS

Methods and any associated references are available in the online version of the paper at http://www.nature.com/natureneuroscience/.

Note: Supplementary information is available on the Nature Neuroscience website.

ACKNOWLEDGMENTS

This work is dedicated to the memory of Dr. Tom Kadesch, an inspirational colleague and mentor. We thank A. West, D. Epstein and members of the Zhou laboratory for critical readings of the manuscript, and the Intellectual and Developmental Disability Research Center Gene Manipulation Core (P30 HD18655) at the Children's Hospital Boston for generation of knockin mice (M. Thompson, Y. Zhou and H. Ye). This work was supported by grants from the US National Institutes of Health (R00 NS058391 and P30 HD026979), the Philadelphia Foundation and International Rett Syndrome Foundation to Z.Z. D.G. acknowledges the generous support of the Alavi-Dabiri Postdoctoral Fellowship. Z.Z. is a Pew Scholar in Biomedical Science.

AUTHOR CONTRIBUTIONS

D.G. designed and performed the EEG and ERP studies, analyzed protein stability, and was involved in most aspects of the project, except for the generation of the mice. M. Allen and I.-T.J.W. characterized mouse phenotypes. L.Z. analyzed protein expression and interaction. M. Amorim analyzed DNA binding and gene expression. A.-R.S.R. and C.O. provided technical assistance. S.C. assisted with targeting construct. L.H. assisted with the generation of T158 antibody. A.M.-B. and J.A.B. helped design and interpret behavioral tests. G.C.C. and S.J.S. helped design and interpret the EEG and ERP studies. Z.Z. generated the knockin mice with supervision from M.E.G., designed the experiments and supervised the project. D.G. and Z.Z. wrote the paper.

COMPETING FINANCIAL INTERESTS

The authors declare no competing financial interests.

Published online at http://www.nature.com/natureneuroscience/.
Reprints and permissions information is available online at http://www.nature.com/reprints/index.html.

1. Amir, R.E. *et al.* Rett syndrome is caused by mutations in X-linked MECP2, encoding methyl-CpG-binding protein 2. *Nat. Genet.* **23**, 185–188 (1999).
2. Bienvenu, T. & Chelly, J. Molecular genetics of Rett syndrome: when DNA methylation goes unrecognized. *Nat. Rev. Genet.* **7**, 415–426 (2006).
3. Chahrour, M. & Zoghbi, H.Y. The story of Rett syndrome: from clinic to neurobiology. *Neuron* **56**, 422–437 (2007).
4. Chen, R.Z., Akbarian, S., Tudor, M. & Jaenisch, R. Deficiency of methyl-CpG binding protein-2 in CNS neurons results in a Rett-like phenotype in mice. *Nat. Genet.* **27**, 327–331 (2001).
5. Guy, J., Hendrich, B., Holmes, M., Martin, J.E. & Bird, A. A mouse Mecp2-null mutation causes neurological symptoms that mimic Rett syndrome. *Nat. Genet.* **27**, 322–326 (2001).
6. Shahbazian, M. *et al.* Mice with truncated MeCP2 recapitulate many Rett syndrome features and display hyperacetylation of histone H3. *Neuron* **35**, 243–254 (2002).
7. Collins, A.L. *et al.* Mild overexpression of MeCP2 causes a progressive neurological disorder in mice. *Hum. Mol. Genet.* **13**, 2679–2689 (2004).
8. Pelka, G.J. Mecp2 deficiency is associated with learning and cognitive deficits and altered gene activity in the hippocampal region of mice. *Brain* **129**, 887–898 (2006).
9. Kerr, B., Alvarez-Saavedra, M., Sáez, M.A., Saona, A. & Young, J.I. Defective body-weight regulation, motor control and abnormal social interactions in Mecp2 hypomorphic mice. *Hum. Mol. Genet.* **17**, 1707–1717 (2008).
10. Samaco, R.C. *et al.* A partial loss of function allele of methyl-CpG-binding protein 2 predicts a human neurodevelopmental syndrome. *Hum. Mol. Genet.* **17**, 1718–1727 (2008).
11. Jentarra, G.M. *et al.* Abnormalities of cell packing density and dendritic complexity in the MeCP2 A140V mouse model of Rett syndrome/X-linked mental retardation. *BMC Neurosci.* **11**, 19 (2010).
12. Guy, J., Gan, J., Selfridge, J., Cobb, S. & Bird, A. Reversal of neurological defects in a mouse model of Rett syndrome. *Science* **315**, 1143–1147 (2007).
13. Lioy, D.T. *et al.* A role for glia in the progression of Rett's syndrome. *Nature* **475**, 497–500 (2011).
14. Ho, K.L. *et al.* MeCP2 binding to DNA depends upon hydration at methyl-CpG. *Mol. Cell* **29**, 525–531 (2008).
15. Dani, V.S. *et al.* Reduced cortical activity due to a shift in the balance between excitation and inhibition in a mouse model of Rett syndrome. *Proc. Natl. Acad. Sci. USA* **102**, 12560–12565 (2005).
16. Dani, V.S. & Nelson, S.B. Intact long-term potentiation but reduced connectivity between neocortical layer 5 pyramidal neurons in a mouse model of Rett syndrome. *J. Neurosci.* **29**, 11263–11270 (2009).
17. Wood, L., Gray, N.W., Zhou, Z., Greenberg, M.E. & Shepherd, G.M.G. Synaptic circuit abnormalities of motor-frontal layer 2/3 pyramidal neurons in an RNA interference model of methyl-CpG-binding protein 2 deficiency. *J. Neurosci.* **29**, 12440–12448 (2009).
18. Uhlhaas, P.J. & Singer, W. Abnormal neural oscillations and synchrony in schizophrenia. *Nat. Rev. Neurosci.* **11**, 100–113 (2010).
19. Gandal, M.J., Edgar, J.C., Klook, K. & Siegel, S.J. Gamma synchrony: towards a translational biomarker for the treatment-resistant symptoms of schizophrenia. *Neuropharmacology* (2011).
20. Roberts, T.P.L. *et al.* MEG detection of delayed auditory evoked responses in autism spectrum disorders: towards an imaging biomarker for autism. *Autism Res.* **3**, 8–18 (2010).
21. Gandal, M.J. *et al.* Validating γ oscillations and delayed auditory responses as translational biomarkers of autism. *Biol. Psychiatry* **68**, 1100–1106 (2010).
22. Chao, H.-T. *et al.* Dysfunction in GABA signaling mediates autism-like stereotypies and Rett syndrome phenotypes. *Nature* **468**, 263–269 (2010).
23. D'Cruz, J.A. *et al.* Alterations of cortical and hippocampal EEG activity in MeCP2-deficient mice. *Neurobiol. Dis.* **38**, 8–16 (2010).
24. Bader, G.G., Witt-Engerström, I. & Hagberg, B. Neurophysiological findings in the Rett syndrome. II. Visual and auditory brainstem, middle and late evoked responses. *Brain Dev.* **11**, 110–114 (1989).
25. Stauder, J.E.A., Smeets, E.E.J., van Mil, S.G.M. & Curfs, L.G.M. The development of visual- and auditory processing in Rett syndrome: an ERP study. *Brain Dev.* **28**, 487–494 (2006).
26. Vacca, M. *et al.* MECP2 gene mutation analysis in the British and Italian Rett Syndrome patients: hot spot map of the most recurrent mutations and bioinformatic analysis of a new MECP2 conserved region. *Brain Dev.* **23** Suppl 1: S246–S250 (2001).
27. Schanen, C. *et al.* Phenotypic manifestations of MECP2 mutations in classical and atypical Rett syndrome. *Am. J. Med. Genet. A.* **126A**, 129–140 (2004).
28. Armstrong, D.D. Neuropathology of Rett syndrome. *J. Child Neurol.* **20**, 747–753 (2005).
29. Feng, G. *et al.* Imaging neuronal subsets in transgenic mice expressing multiple spectral variants of GFP. *Neuron* **28**, 41–51 (2000).
30. Shahbazian, M.D., Antalffy, B., Armstrong, D.L. & Zoghbi, H.Y. Insight into Rett syndrome: MeCP2 levels display tissue- and cell-specific differences and correlate with neuronal maturation. *Hum. Mol. Genet.* **11**, 115–124 (2002).
31. Skene, P.J. *et al.* Neuronal MeCP2 is expressed at near histone-octamer levels and globally alters the chromatin state. *Mol. Cell* **37**, 457–468 (2010).
32. Chahrour, M. *et al.* MeCP2, a key contributor to neurological disease, activates and represses transcription. *Science* **320**, 1224–1229 (2008).
33. Nan, X., Tate, P., Li, E. & Bird, A. DNA methylation specifies chromosomal localization of MeCP2. *Mol. Cell. Biol.* **16**, 414–421 (1996).
34. Nuber, U.A. *et al.* Up-regulation of glucocorticoid-regulated genes in a mouse model of Rett syndrome. *Hum. Mol. Genet.* **14**, 2247–2256 (2005).
35. Jones, P.L. *et al.* Methylated DNA and MeCP2 recruit histone deacetylase to repress transcription. *Nat. Genet.* **19**, 187–191 (1998).
36. Nan, X. *et al.* Transcriptional repression by the methyl-CpG-binding protein MeCP2 involves a histone deacetylase complex. *Nature* **393**, 386–389 (1998).
37. Uhlhaas, P.J., Pipa, G., Neuenschwander, S., Wibral, M. & Singer, W. A new look at gamma? High- (>60 Hz) γ-band activity in cortical networks: function, mechanisms and impairment. *Prog. Biophys. Mol. Biol.* **105**, 14–28 (2011).
38. Tallon-Baudry, C. & Bertrand, O. Oscillatory gamma activity in humans and its role in object representation. *Trends Cogn. Sci.* **3**, 151–162 (1999).
39. Buzsáki, G. & Draguhn, A. Neuronal oscillations in cortical networks. *Science* **304**, 1926–1929 (2004).
40. Winterer, G. *et al.* Schizophrenia: reduced signal-to-noise ratio and impaired phase-locking during information processing. *Clin. Neurophysiol.* **111**, 837–849 (2000).
41. Foster, B.A., Coffey, H.A., Morin, M.J. & Rastinejad, F. Pharmacological rescue of mutant p53 conformation and function. *Science* **286**, 2507–2510 (1999).
42. Kishi, N. & Macklis, J.D. MECP2 is progressively expressed in post-migratory neurons and is involved in neuronal maturation rather than cell fate decisions. *Mol. Cell. Neurosci.* **27**, 306–321 (2004).
43. Uhlhaas, P.J. & Singer, W. Neural synchrony in brain disorders: relevance for cognitive dysfunctions and pathophysiology. *Neuron* **52**, 155–168 (2006).
44. Ben-Ari, Y. Developing networks play a similar melody. *Trends Neurosci.* **24**, 353–360 (2001).

ONLINE METHODS

Generation of *Mecp2*$^{T158A/y}$ and *Mecp2*$^{loxP/y}$ mice. The targeting construct used for homologous recombination in ES cells was cloned in two arms by PCR amplification of sv129 genomic DNA. The 5′ arm was PCR amplified with 5′-AGGAGGTAGGTGGCATCCTT-3′ and 5′-CGTTTGATCACCATGAC CTG-3′ primers, whereas the 3′ arm was PCR amplified with 5′-GAAATGGC TTCCCAAAAAGG-3′ and 5′-AAAACGGCACCCAAAGTG-3′ primers. Restriction sites at the ends of each arm were created using nested primers for cloning into a vector containing a *loxP*-flanked neomycin cassette (Neo) and a diphtheria toxin A negative-selection cassette. Threonine 158 was mutated to alanine in MeCP2 using QuikChange (Stratagene) site-directed mutagenesis. A single nucleotide at codon T160 also underwent site-directed mutagenesis for a silent mutation to introduce a BstEII restriction site to correctly identify targeted ES cells.

The targeting construct was confirmed by sequencing, linearized using NotI and subsequently electroporated into sv129 mouse ES cells. Two MeCP2 T158A ES cell clones and two *loxP* ES cell clones were independently injected into C57BL/6 blastocysts and subsequently implanted into pseudopregnant females. The resulting chimeric offspring were mated with C57BL/6 *EIIa-cre* mice for embryonic deletion of the Neo cassette, and the agouti offspring were screened by PCR genotyping to confirm germ line transmission of the *T158A* or *loxP* allele.

Animal husbandry. Experiments were conducted in accordance with the ethical guidelines of the US National Institutes of Health and with the approval of the Institutional Animal Care and Use Committee of the University of Pennsylvania. All of the experiments described were performed using mice on a congenic sv129:C57BL/6 background with the mutation backcrossed to C57BL/6 mice (Charles River) for at least five generations, unless otherwise stated. Mice were genotyped using a PCR-based strategy to detect the residual *loxP* sequence remaining in intron III after Cre-mediated excision of the neomycin cassette. The genotyping primers (5′-GGATTGTGGAAAAGCCAG-3′ and 5′-ATGACCTGGGCAGATGTGGTAG-3′) give rise to a 620-bp product from the wild-type allele and 691 bp for the *T158A* allele.

Cell cultures. Cortical cultures were prepared from E16 mouse embryos similar to that previously described[45]. For analysis of protein stability, cultures were treated with vehicle (DMSO) or 100 μM CHX (Sigma) for 3, 6 or 9 h before lysis in 1× SDS sample buffer. Human fibroblast cells were obtained from the Coriell Institute and cultured as recommended.

Quantitative western analysis. Quantitative western blot was performed using Odyssey Infrared Imaging System (Licor). For primary antibodies, we used a rabbit polyclonal antibody directed to the C-terminal of MeCP2 (1:1,000)[46], mouse antibody to NeuN (1:500, Chemicon) and rabbit antibody to histone H3 (1:10,000, Upstate). For secondary antibodies, we used antibodies to rabbit IRDye 680LT and mouse IRDye 800CW (Licor). Quantification of protein expression levels was carried out following Odyssey Infrared Imaging System protocols. Full-length blots are presented in **Supplementary Figure 13**.

Quantitative RT-PCR. For measurements of gene expression in brain tissues, total RNA was isolated using Trizol reagent (Invitrogen) and treated with TURBO DNase (Ambion). We reverse transcribed 1 μg of total RNA by oligo-dT priming using SuperScriptIII reverse transcriptase (Invitrogen). Quantitative real-time PCR was performed on 10 ng of the resulting cDNA using SYBR Green detection (Applied Biosystems). All quantitative PCR primer pairs are exon-spanning and are available on request. All mRNA levels of genes of interest were normalized to *β-tubulin III* mRNA levels.

Immunohistochemistry. Mice were anesthetized with 1.25% Avertin (wt/vol), transcardially perfused with 4% paraformaldehyde (wt/vol), and postfixed overnight at 4 °C. Immunohistochemistry was performed on 20-μm free-floating sections as previously described[47]. Tissues were incubated with primary antibodies in blocking solution (rabbit antibody to total MeCP2, 1:1,000) overnight at 4 °C. Fluorescence detection was performed using antibody to rabbit conjugated to Alexa Fluor-488 (2.67 μg ml^{-1}, Invitrogen) for 1 h at 22–24 °C. Sections were counterstained with TOPRO-3 (1:1,000; Invitrogen) to visualize DNA. Images were acquired using a Leica confocal microscope. Images were acquired using identical settings for laser power, detector gain amplifier offset and pinhole diameter in each channel.

ChIP. Mouse forebrain tissues were homogenized in cross-linking buffer (1% formaldehyde (wt/vol), 100 mM HEPES (pH 7.5), 100 mM NaCl, 1mM EDTA, 1 mM EGTA) and cross-linked for 10 min at 22–24 °C. After quenching with 125 mM glycine, cross-linked tissue was washed with ice-cold PBS and dounced 12 strokes in lysis buffer (50 mM HEPES (pH 7.5), 140 mM NaCl, 1 mM EDTA, 1 mM EGTA, 10% glycerol (vol/vol), 0.5% NP-40 (vol/vol), and 0.25% Triton X-100 (vol/vol) with protease inhibitors). Nuclei were pelleted, washed and resuspended in chromatin buffer (10 mM Tris-HCl (pH 8.0), 1 mM EDTA, and 0.5 mM EGTA with protease inhibitors). Sonication was performed to break chromatin into sizes ranging from 400 bp to 2 kb. Salt and detergent were added to adjust the chromatin buffer to 0.5% Triton X-100, 150 mM NaCl, 10 mM EDTA, and 10% sodium deoxycholate (DOC, vol/vol). For immunoprecipitation, rabbit polyclonal antisera directed against total MeCP2 (5 μl) was coupled to 10 μl of Protein A Dynabeads (Invitrogen) in the absence or presence of 1 μg of the peptide from which antisera was raised (for a peptide blocking control). ChIP was performed at 4 °C overnight. Precipitated chromatins were washed six times with wash buffer (10 mM Tris (pH 8.0), 320 mM LiCl, 10 mM EDTA, 0.5% Triton X-100, and 0.1% DOC with protease inhibitors). Chromatin was eluted twice with elution buffer (50 mM Tris-HCl (pH 8.0), 10 mM EDTA, and 1% SDS, wt/vol), digested with proteinase K (0.5 mg ml^{-1}) and reverse-crosslinked at 65 °C overnight. After RNAse A treatment, DNA fragments were extracted with phenol/chloroform, precipitated with ethanol, and purified with a Qiaquick PCR purification column. The amount of DNA fragments of interest in ChIPs was measured by quantitative real-time PCR using SYBR green detection. All quantitative PCR primer sequences are available on request.

EEG surgery. Mice underwent stereotaxic implantation of tripolar electrode assemblies (PlasticsOne) for nonanesthetized recording of auditory ERPs. Mice were anesthetized with isoflurane (4% for induction (vol/vol), 1.5–2% for surgery with 1 l min^{-1} O_2). Three stainless steel electrodes, mounted in a single pedestal were aligned to the sagittal axis of the skull. A stainless steel recording electrode was placed 2.0 mm posterior, 2.0 mm left lateral relative to bregma and 1.8 mm depth (**Supplementary Fig. 14**). Ground and reference electrodes were placed anterior of the hippocampal electrode at 1.0 mm and 2.0 mm distances, respectively. The electrode pedestal was secured to the skull with ethyl cyanoacrylate and dental cement. Post-operative analgesia was supplied using the opioid analgesic, buprenorphine (buprenex, subcutaneous, 0.1 μg per g of body weight). Mice were allowed to recover for 7 d before EEG recordings.

EEG recordings. EEG recordings were performed on freely mobile, nonanesthetized mice in their home cage environment after a 20-min acclimation to the recording room. Recordings were performed using Spike2 software connected to a Power 1401 II interface module (CED) and high impedance differential AC amplifier (A-M Systems). Signals were acquired at 1,667 Hz and band-pass filtered between 1 and 500 Hz with a 60-Hz notch filter and gain of 1,000.

ERPs were recorded by presentation of auditory stimuli consisting of a series of 250 white-noise clicks of 10-ms duration, 85-dB sound pressure and 4-s interstimulus intervals. Stimuli were presented through speakers on the recording chamber ceiling (Model 19-318A, 700–10,000 Hz frequency response, Radio Shack) connected to a digital audio amplifier (RCA Model STAV3870, Radio Shack). ERP traces were generated by averaging across single trial epochs centered at $t = 0 \pm 2$ s. Single trials were baseline corrected by subtracting the temporal mean at $t = -1$ s to $t = 0.5$ s. Altering the baseline closer to sound presentation had no effect on the results shown. The mean ERP amplitudes were subsequently calculated across 250 trials.

Time-frequency analysis of EEG. For each recording in which mice were presented with 250 white-noise clicks (10-ms duration, 85-dB sound pressure, 4-s interstimulus intervals), we computed event-related power and phase as a function of frequency and time. Event-related power changes and phase locking were determined similar to that described previously[38,48]. EEG signal was filtered into bands with center frequencies ranging from 2–140 Hz in 1-Hz steps

doi:10.1038/nn.2997

and 2-Hz bandwidths. The raw signal was filtered using a two-way least-squares finite impulse response filter. The Hilbert transform was applied to create a complex-valued time series

$$V(t) = v(t) + iu(t)$$

where the real part, $v(t)$, is the same as the normalized filtered EEG and the imaginary part, $u(t)$, is from the Hilbert transform of $v(t)$, given by

$$u(t) = \frac{1}{\pi} PV \int_{-\infty}^{+\infty} \frac{V(t')}{(t - t')} dt'$$

and PV signifies the Cauchy principal value. Analytic power, $P(f,t)$, as a function of frequency f and time t is given by

$$P(f,t) = v(f,t)^2 + u(f,t)^2$$

We determined changes in event-related power by isolating single trial epochs of 4-s duration with $t = 0$ representing sound presentation ±2 s. We determined power response relative to the prestimulus basis for each trial. We used a baseline of the mean power at $t = -1$ s to $t = 0.5$ s. Altering the baseline period did not affect the conclusions of the study. The mean power across the 250 trials was subsequently calculated.

The instantaneous phase time series, $\theta(f,t)$, was determined as a function of time and frequency by taking the two-argument four quadrant arctangent (atan2) of the real parts of $v(t)$ and $u(t)$ such that phase values were in the range from $-\pi$ to π.

$$\theta(f,t) = 2\arctan\frac{u(f,t)}{\sqrt{v(f,t)^2 + u(f,t)^2} + v(f,t)}$$

An example of EEG amplitudes and phase calculated using this method for 1-s epoch of EEG recorded in a P90 wild-type mouse is shown (**Supplementary Fig. 15**). Event-related phase locking was measured using a PLF by calculating 1 – circular variance of instantaneous phase measurements, defined as

$$PLF = 1 - \frac{1}{n}\sqrt{\sum_{k=1}^{n}(\cos\theta_k)^2 + \sum_{k=1}^{n}(\sin\theta_k)^2}$$

Basal EEG power measurement. Basal EEG power was determined across a 60-s period during a period of wakefulness, as assessed by behavioral monitoring of mice. For each 60-s recording, we computed the power as a function of frequency and time with frequency varying between 2 and 140 Hz using 1-Hz increments. To measure the power at frequency f, we filtered the data between $f \pm 1$ Hz, then calculated power using the Hilbert transform as described above. The power for each 60-s recording was calculated as the mean power across individual 1-s epochs during this 60-s period. The relative power at each individual frequency was presented as a fraction of the sum of powers at all frequencies. These relative powers were then separated into frequency bins and calculated as the area under the curve. Relative power measurements for *Mecp2*$^{T158A/y}$ or *Mecp2*$^{-/-}$ were then expressed as a percentage of wild type.

Auditory brainstem response (ABR) recordings. ABR recordings were performed using the same equipment and electrode placement as other recordings, except that EEG signals were acquired at 15,625 Hz. Auditory stimulation consisted of 4,000 white-noise clicks of 3-ms duration with a 125-ms interstimulus interval at seven sound pressures: decreasing from 85 to 55 dB. The EEG signal was digitally filtered between 100 and 500 Hz and EEG amplitudes averaged across trials centered at $t = 0$ s representing sound presentation. The average ABR consists of five amplitude peaks and the amplitudes of these peaks decrease with decreasing sound pressure[49].

Behavioral assays. All behavioral studies were carried out blinded to genotype where possible. Because of the presence of overt RTT-like symptoms in *Mecp2*$^{T158A/y}$ and *Mecp2*$^{-/y}$ mice, the identity of the genotype was sometimes noticeable, but care was taken to avoid bias. For all studies, the mice were allowed to habituate to the testing room for 30 min before the test and testing was performed at the same time of day.

Phenotypic scoring. Phenotypic scoring was performed on a weekly basis for the absence or presence of RTT-like symptoms as described previously[12].

Locomotor assay. Locomotor activity was measured by beam breaks in a photobeam frame (Med Associates). Mice were placed into a clean home cage–like environment lined with bedding and resting in a photobeam frame. The number of beam breaks as a measure of locomotor activity was quantified over 5 min.

Accelerating rotarod. At approximately 9 weeks of age, mice were placed on an accelerating rotarod apparatus (Med Associates) for 16 trials (four trials a day on four consecutive days) with at least 15 min of rest between the trials. Each trial lasted for a maximum of 5 min, during which the rod accelerated linearly from 3.5 to 35 rpm. The amount of time and rpm for each mouse to fall from the rod was recorded for each trial.

Elevated zero maze. The elevated zero maze was performed by placing mice in one of the closed quadrants and their movement traced over the course of 5 min. Analysis was performed with TopScan software (Clever Systems).

Fear conditioning. Mice were placed in individual chambers (Med Associates) for 2 min followed by a loud tone (85 dB, 2 kHz) for 20 s, co-terminating with a 2-s, 0.75-mA foot shock. Mice were left undisturbed for 1 min, after which a second pairing of sound cue and shock was delivered. Mice were returned to their home cage 90 s after the second shock. Freezing behavior, defined as no movement except for respiration, was determined before and after the tone-shock pairings and scored by FreezeScan NI version 2.00. To test for context-dependent learning, we placed mice back into the same testing boxes 24 h later without a tone or shock for 5 min. The mice were placed into a novel chamber 1 h later and tested for cued fear memory. The cue tone (85 dB, 2 kHz) was played for 1 min, 2 min after entering the chamber.

Open field. At the beginning of each trial, the subject was placed in the center of the open-field apparatus and the subject's behavior was videotaped for the duration of the trial. The total number of line crossings for each trial was recorded over a 5-min testing period.

Statistics. Statistics were performed using Prism 5.0 (GraphPad Software). Individual statistical tests performed are listed in the figure legends. A P value < 0.05 was considered to be significant and Bonferroni or Tukey *post hoc* tests were performed where appropriate to correct for multiple hypothesis testing. Tests for normality were performed where necessary using the D'Agostino-Pearson omnibus test.

45. Goffin, D. *et al.* Dopamine-dependent tuning of striatal inhibitory synaptogenesis. *J. Neurosci.* **30**, 2935–2950 (2010).
46. Zhou, Z. *et al.* Brain-specific phosphorylation of MeCP2 regulates activity-dependent Bdnf transcription, dendritic growth, and spine maturation. *Neuron* **52**, 255–269 (2006).
47. Liao, W.-L. *et al.* Modular patterning of structure and function of the striatum by retinoid receptor signaling. *Proc. Natl. Acad. Sci. USA* **105**, 6765–6770 (2008).
48. Canolty, R.T. *et al.* High gamma power is phase-locked to theta oscillations in human neocortex. *Science* **313**, 1626–1628 (2006).
49. Hardisty-Hughes, R.E., Parker, A. & Brown, S.D.M. A hearing and vestibular phenotyping pipeline to identify mouse mutants with hearing impairment. *Nat. Protoc.* **5**, 177–190 (2010).

SUPPLEMENTARY INFORMATION

Rett Syndrome Mutation MeCP2 T158A Disrupts DNA Binding, Protein Stability and ERP Responses

Darren Goffin, Megan Allen, Le Zhang, Maria Amorim, I-Ting Judy Wang, Arith-Ruth S. Reyes, Amy Mercado-Berton, Caroline Ong, Sonia Cohen, Linda Hu, Julie A. Blendy, Gregory C. Carlson, Steve J. Siegel, Michael E. Greenberg and Zhaolan (Joe) Zhou

Figure S1

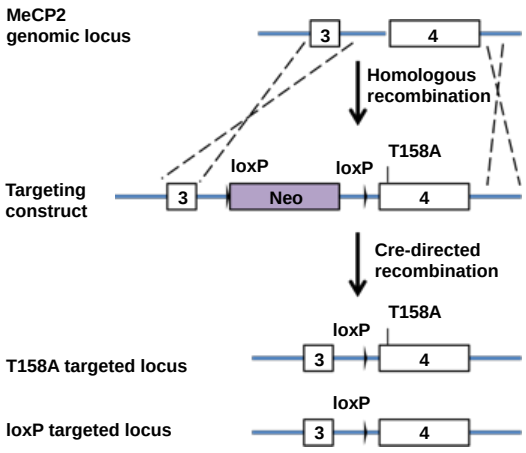

Supplementary Figure 1: Generation of MeCP2 T158A and loxP knockin mice

Targeting strategy to generate MeCP2 T158A and loxP knockin mice. The genomic region surrounding *Mecp2* exons III and IV was targeted for homologous recombination using a construct in which the floxed neomycin positive selection cassette (Neo) was inserted in a non-conserved region of intron III. The location of the mutation in exon IV to create T158A is indicated. Since we were testing for the effects of a single nucleotide mutation, two lines of mice were generated: those with and those without the T158A mutation. Both lines contained floxed loxP sites. Following production of chimera, the Neo cassette was removed using *EIIa-cre* mice. The targeted alleles after cre-mediated removal of the Neo cassette are illustrated.

Nature Neuroscience: doi:10.1038/nn.2997

Figure S2

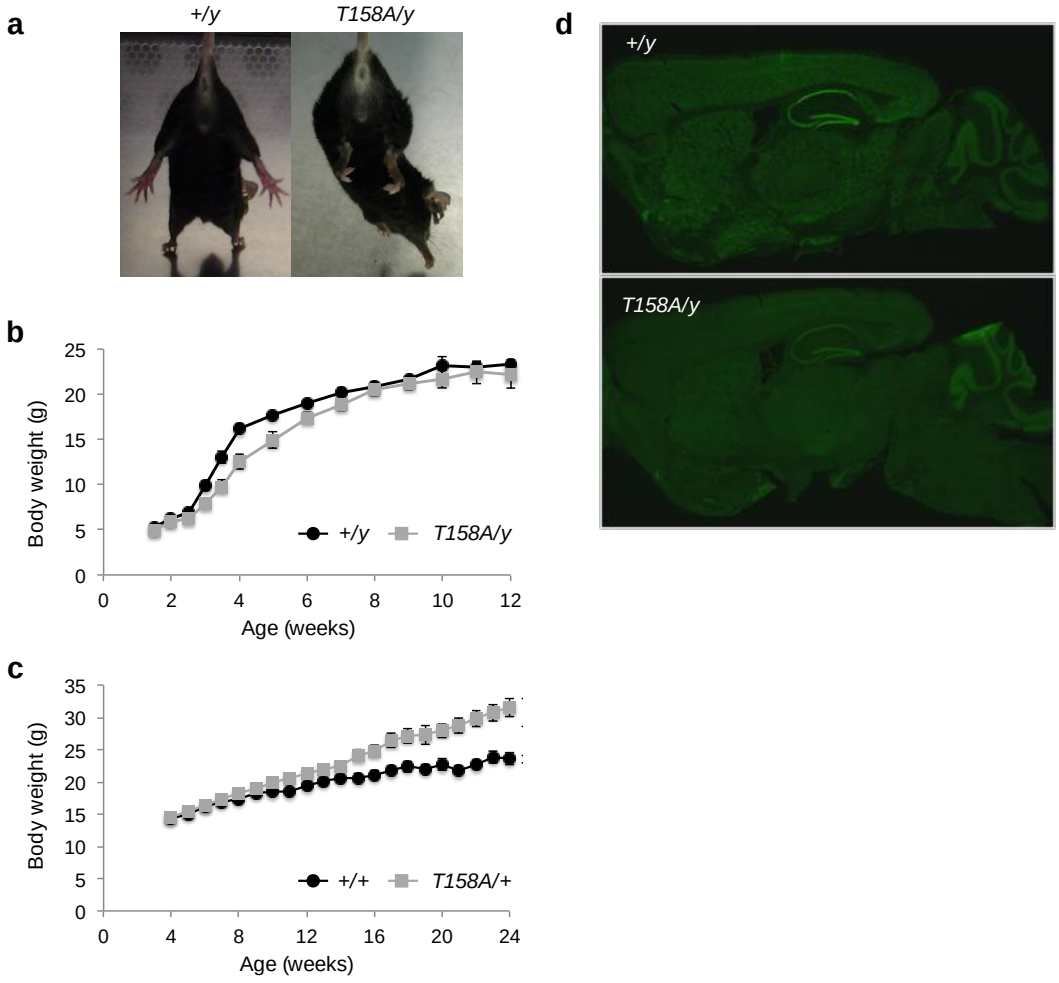

Supplementary Figure 2: Characterization of MeCP2 T158A mice

a. Stereotypical hindlimb clasping upon tail suspension in an *Mecp2*$^{T158A/y}$ mouse at 13 weeks of age versus an age-matched *Mecp2*$^{+/y}$ littermate. **b.** Body weights in male *Mecp2*$^{T158A/y}$ mice (n = 11; $F_{1,252}$ = 27.75, p<0.0001, two-way ANOVA) compared to WT littermates (n = 9). Points represent mean ± SEM. **c.** Body weights in female *Mecp2*$^{T158A/+}$ mice (n = 7; $F_{1,242}$ = 176.77, p<0.0001, two-way ANOVA) compared to *Mecp2*$^{+/+}$ littermates (n = 7). Points represent mean ± SEM. **d.** Normal gross brain anatomy in *Mecp2*$^{T158A/y}$ mice compared to *Mecp2*$^{+/y}$ mice. Sagittal sections were stained with an antibody against MeCP2.

Nature Neuroscience: doi:10.1038/nn.2997

Figure S3

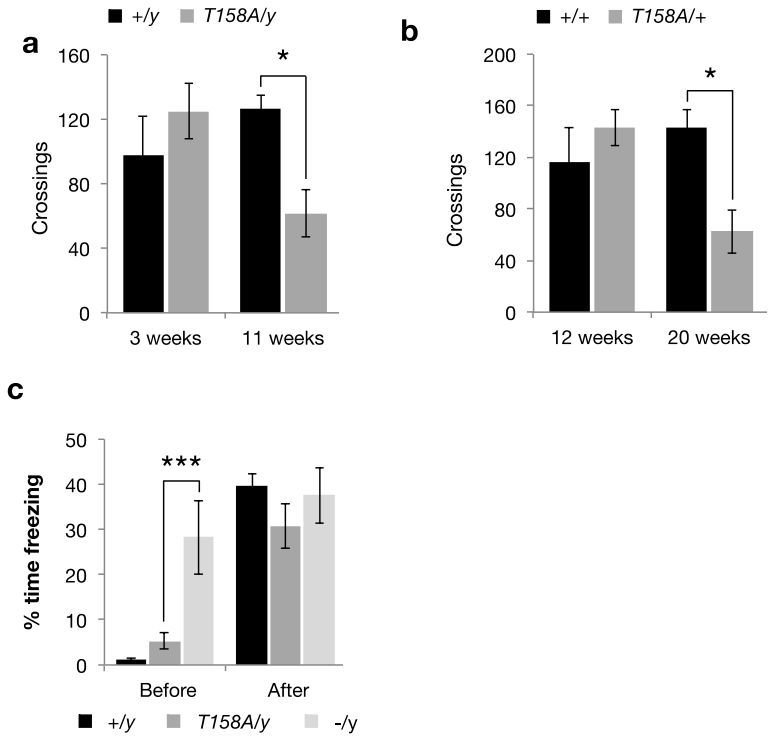

Supplementary Figure 3: Behavioral phenotypes of *Mecp2*$^{T158A/y}$ mice

a. Locomotor activity measured in male mice using an open field assay at 11 and 3 weeks of age. Bars represent mean ± SEM (n = 6 for *Mecp2*$^{+/y}$ and n = 8 for *Mecp2*$^{T158A/y}$). * *p*-value < 0.05; two-tailed t-test with Bonferroni correction. **b.** Locomotor activity measured in female mice using an open field assay at 20 and 12 weeks of age. Bars represent mean ± SEM (n = 5 for *Mecp2*$^{+/+}$ and n = 5 for *Mecp2*$^{T158A/+}$). * *p*-value < 0.05; two-tailed t-test with Bonferroni correction. **c.** Percentage time spent freezing in *Mecp2*$^{+/y}$ (n = 33), *Mecp2*$^{T158A/y}$ (n = 16) and *Mecp2*$^{-/y}$ mice (n = 12) prior to, and subsequent to tone and shock on training day of fear conditioning procedure. *Mecp2*$^{-/y}$ mice freeze significantly more than WT or *Mecp2*$^{T158A/y}$ mice prior to experimentation obviating them from further analysis. Bars represent mean ± SEM. *** *p*-value < 0.001; two-tailed t-test with Bonferroni correction.

Nature Neuroscience: doi:10.1038/nn.2997

Figure S4.

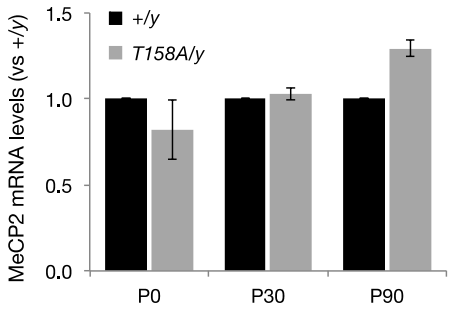

Supplementary Figure 4: MeCP2 mRNA expression is not affected by T158A mutation

MeCP2 mRNA levels in *Mecp2*$^{T158A/y}$ mice (n = 3) at P0, P30 or P90 compared to *Mecp2*$^{+/y}$ littermates (n = 3). Bars represent mean ± SEM. Statistics performed using one-sample t-tests.

Nature Neuroscience: doi:10.1038/nn.2997

Figure S5

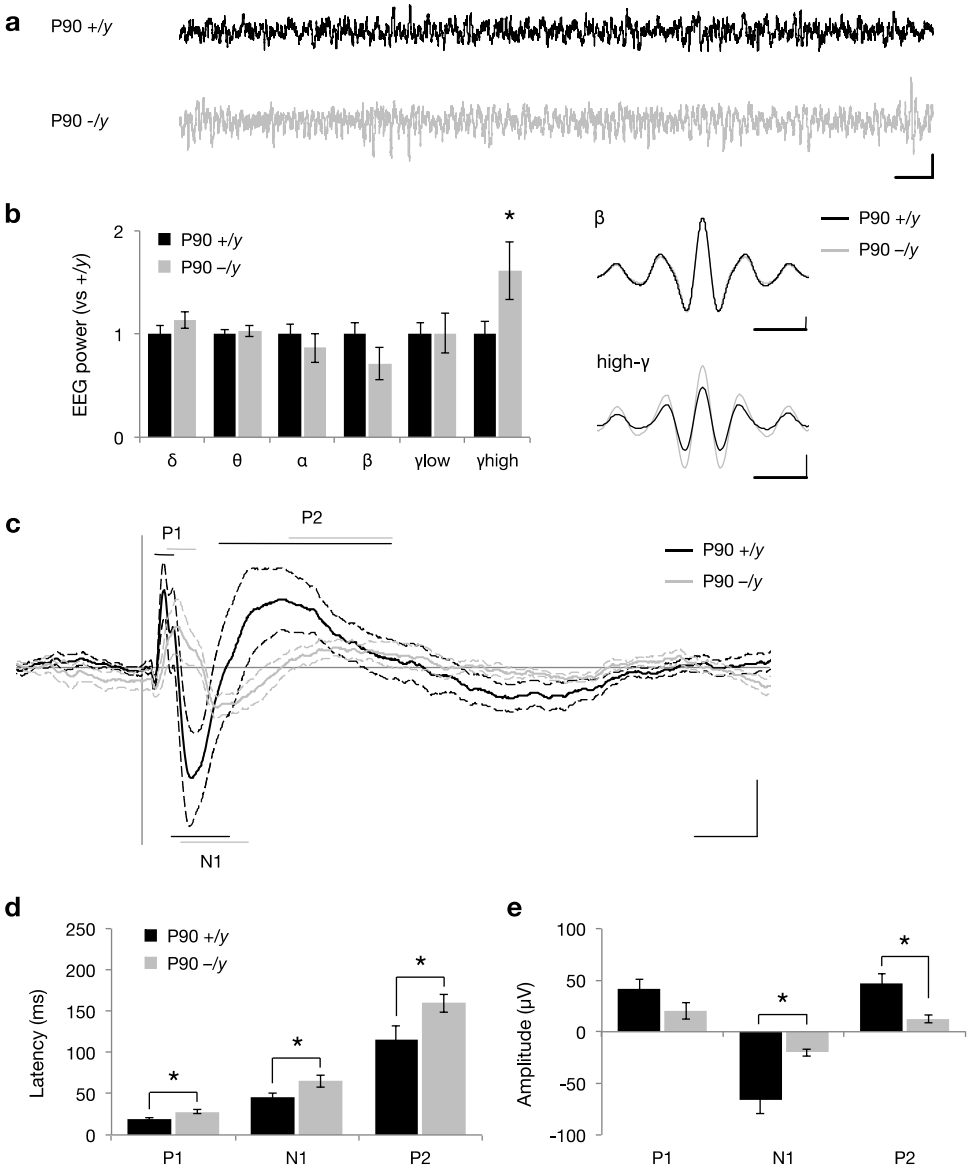

Supplementary Figure 5: ***Mecp2*-null mice exhibit alterations in auditory-evoked ERPs**

a. Representative EEG traces of awake, freely mobile mice. Scale bar corresponds to 1 second (horizontal) and 200 μA (vertical). **b.** Basal EEG power measurements in *Mecp2*$^{-/y}$ mice (n = 8) and *Mecp2*$^{+/y}$ littermates (n = 8). Bars represent mean ± SEM. * *p*-value < 0.05; two-tailed t-test with Bonferroni correction. Insets show β and high-γ mean amplitudes across EEG recordings. Scale bars represent one oscillation cycle (horizontal) and 20 μA (vertical). **c.** Grand average ERPs following 85-dB sound presentation. Traces represent mean amplitude (solid line) ± SEM (dashed lines). The characteristic polarity peaks P1, N1 and P2 are highlighted with straight lines with the length indicating latency range. Scale bar corresponds to 50 ms (horizontal) and 20 μA (on vertical). **d.** Latencies and **e.** amplitudes of ERP peaks. Bars represent mean ± SEM. * *p*-value < 0.05; two-tailed t-test with Bonferroni correction.

Nature Neuroscience: doi:10.1038/nn.2997

Figure S6

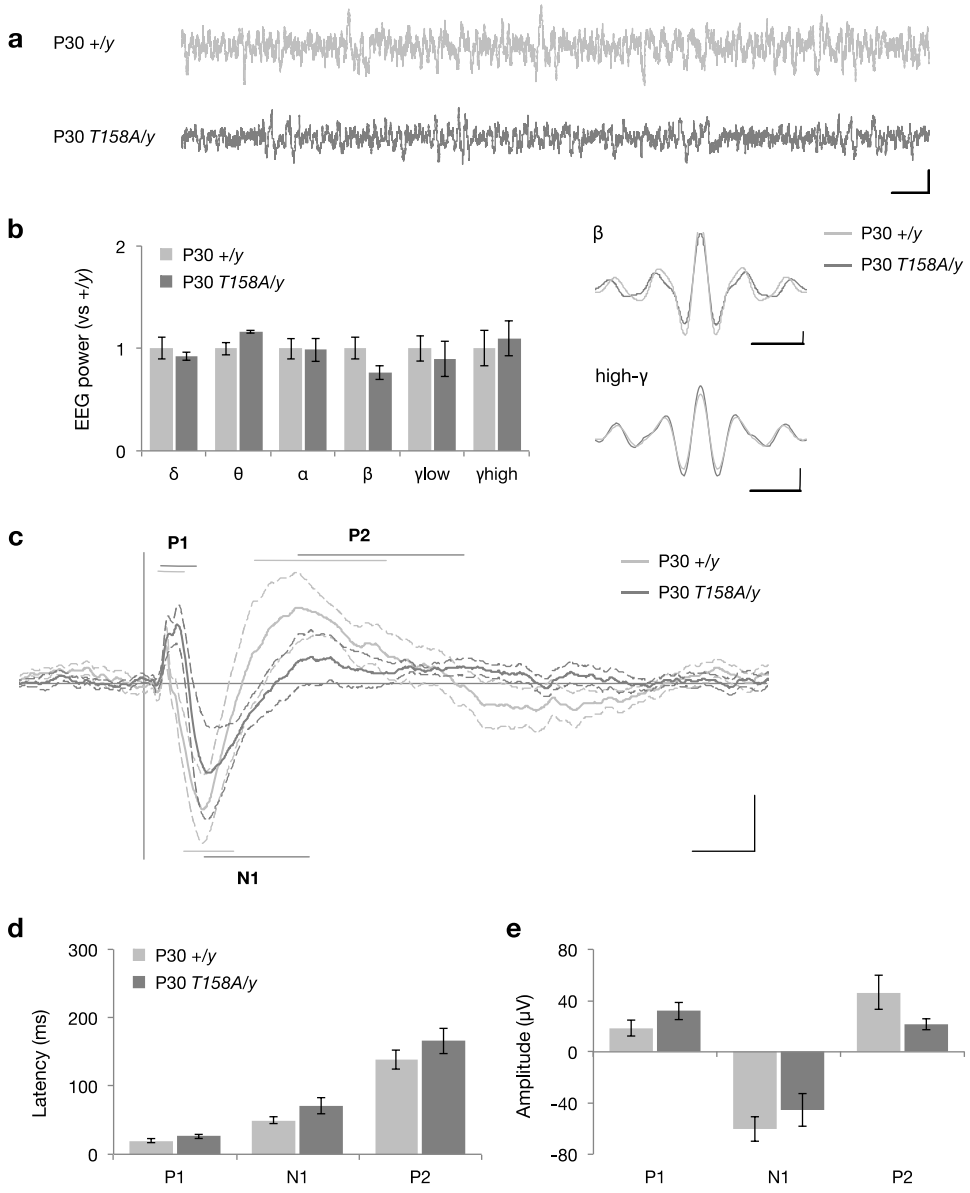

Supplementary Figure 6: Auditory-evoked ERPs are not affected in *Mecp2*$^{T158A/y}$ mice at P30

a. Representative EEG traces of awake, freely mobile mice. Scale bar corresponds to 1 second (horizontal) and 200 μA (vertical). **b.** Basal EEG power measurements in P30 *Mecp2*$^{T158A/y}$ mice (n = 7) and *Mecp2*$^{+/y}$ littermates (n = 8). Bars represent mean ± SEM. * *p*-value < 0.05; two-tailed t-test with Bonferroni correction. Insets show β and high-γ mean amplitudes across EEG recordings. Scale bars represent one oscillation cycle (horizontal) and 20 μA (vertical). **c.** Grand average ERPs following 85-dB sound presentation. Traces represent mean amplitude (solid line) ± SEM (dashed lines). The characteristic polarity peaks P1, N1 and P2 are highlighted with straight lines with the length indicating latency range. Scale bar corresponds to 50 ms (horizontal) and 20 μA (on vertical). **d.** Latencies and **e.** amplitudes of ERP peaks. Bars represent mean ± SEM. Statistics performed using two-tailed t-tests with Bonferroni correction.

Nature Neuroscience: doi:10.1038/nn.2997

Figure S7

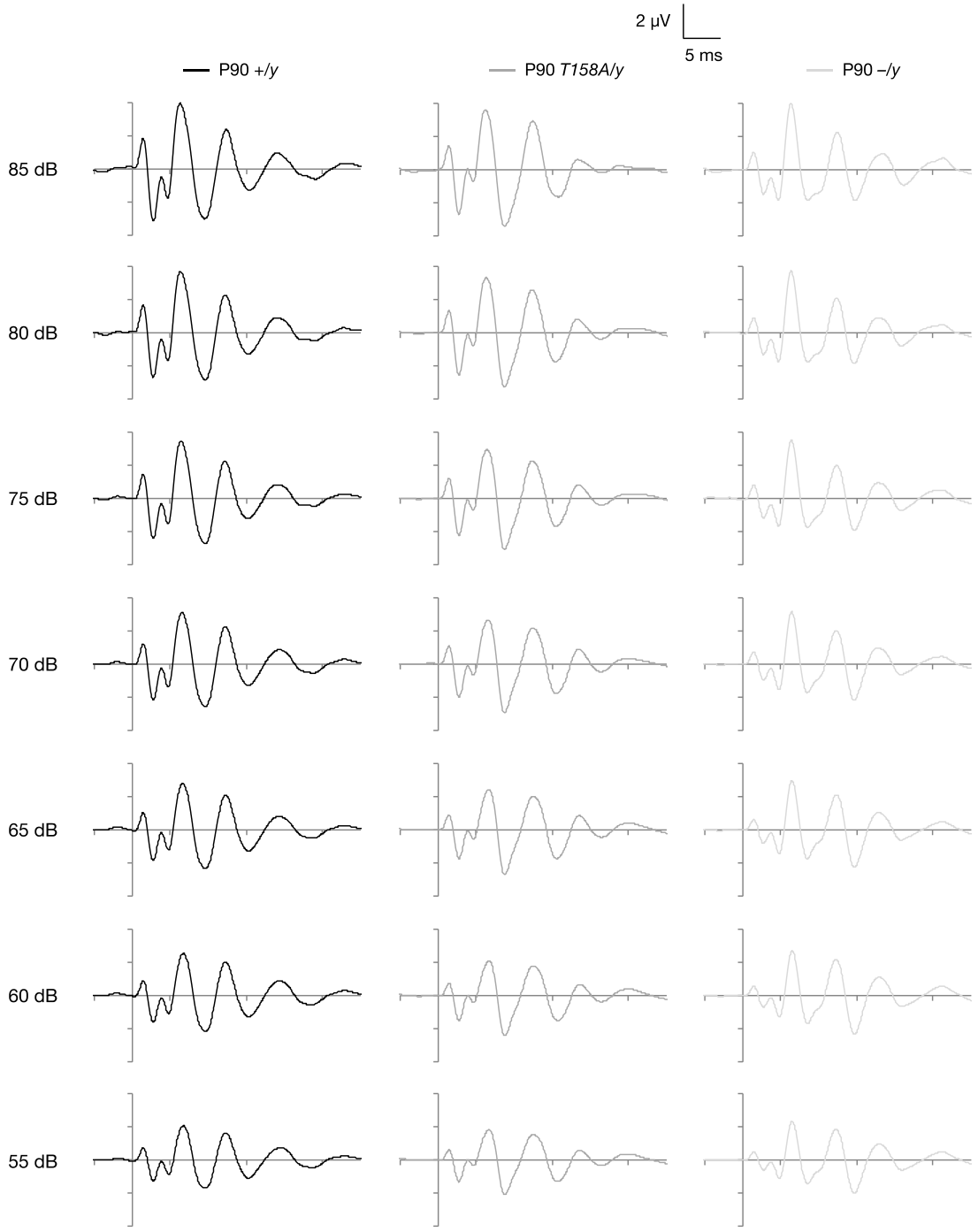

Supplementary Figure 7: Auditory brainstem responses

Auditory brain stem responses from P90 *Mecp2*$^{+/y}$, *Mecp2*$^{T158A/y}$ and *Mecp2*$^{-/y}$ mice. Mice were presented with 4,000 white-noise clicks (3 ms duration, 125 ms inter-stimulus interval) ranging from 85-dB to 55 dB sound pressures. ABR responses decreased to a similar extent in all three genotypes with decreasing sound pressure.

Nature Neuroscience: doi:10.1038/nn.2997

Figure S8

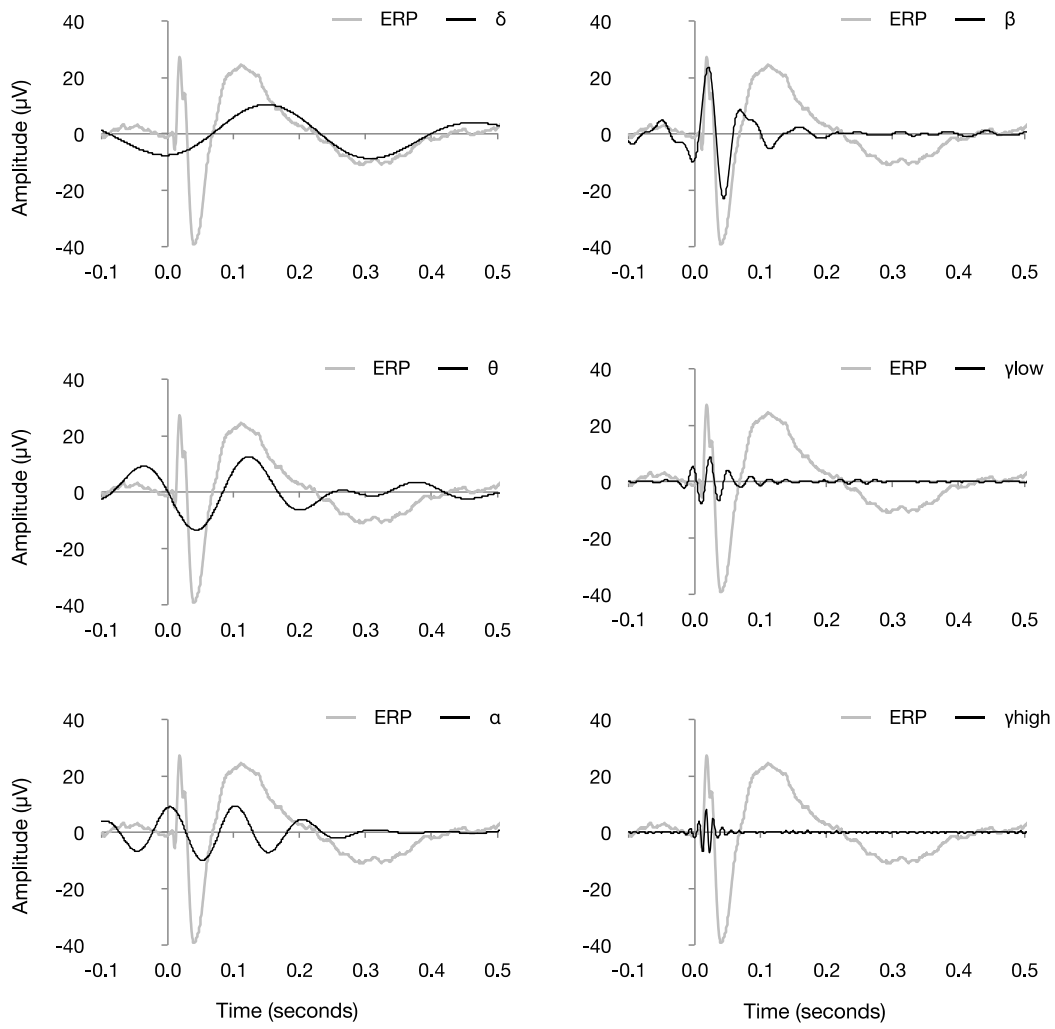

Supplementary Figure 8: Oscillation changes occur for multiple cycles during ERPs

EEG traces were band pass filtered in frequency ranges defined as δ (2-4 Hz), θ (4-8 Hz), α (8-12 Hz), β (12-30 Hz), γlow (30-50 Hz) and γhigh (70-140 Hz). The P1 peak consists primarily of oscillations in the β, low- and high-γ ranges. The N1 peak is composed primarily of α and β frequencies. The P2 peak is primarily composed of δ and θ frequencies.

Nature Neuroscience: doi:10.1038/nn.2997

Figure S9

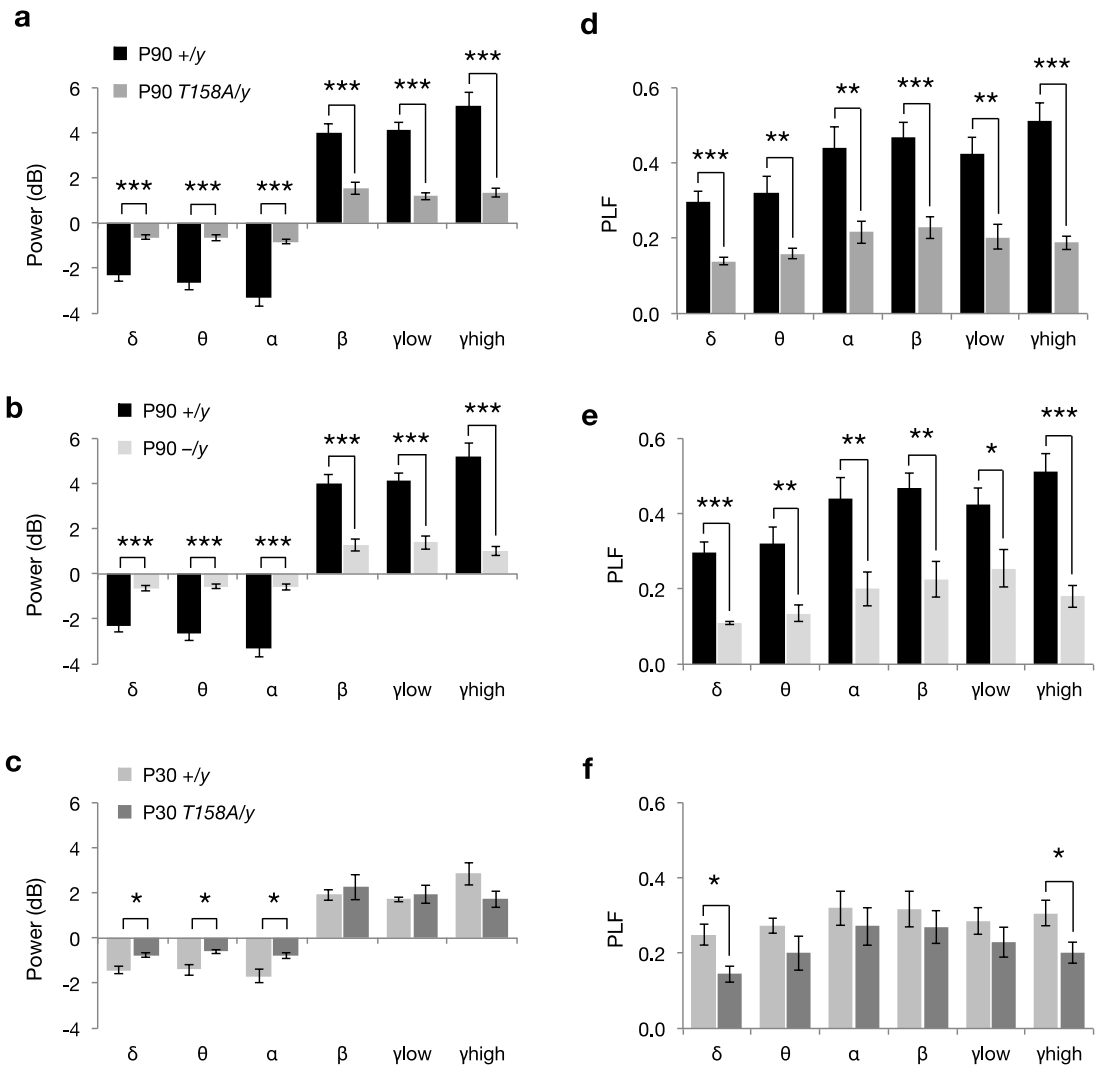

Supplementary Figure 9: Quantification of event-related power and PLF changes

a. Event-related power changes in *Mecp2*$^{T158A/y}$ mice and *Mecp2*$^{+/y}$ littermates at P90. **b.** Event-related power changes in *Mecp2*$^{-/y}$ mice and *Mecp2*$^{+/y}$ littermates at P90. **c.** Event-related power changes in *Mecp2*$^{T158A/y}$ mice and *Mecp2*$^{+/y}$ littermates at P30. **d.** Event-related PLF in *Mecp2*$^{T158A/y}$ mice and *Mecp2*$^{+/y}$ littermates at P90. **e.** Event-related PLF in *Mecp2*$^{-/y}$ mice and *Mecp2*$^{+/y}$ littermates at P90. **f.** Event-related PLF in *Mecp2*$^{T158A/y}$ mice and *Mecp2*$^{+/y}$ littermates at P30. Bars represent mean ± SEM. * p-value < 0.05, ** < 0.01 and *** < 0.001; two-tailed t-test with Bonferroni correction.

Nature Neuroscience: doi:10.1038/nn.2997

Figure S10

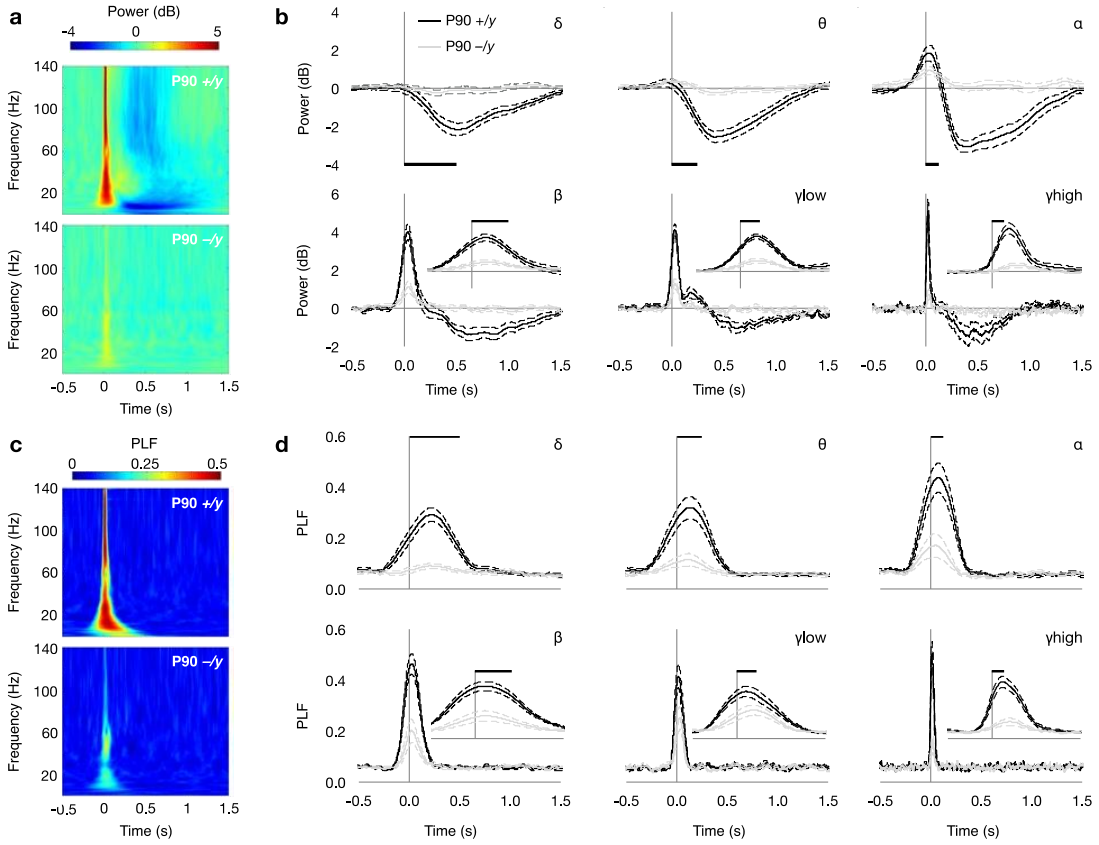

Supplementary Figure 10: Time-frequency analysis in *Mecp2*$^{-/y}$ mice

a. Time-frequency plots showing event-related power in response to 85-dB white-noise clicks. Time is plotted on the abscissa (where $t = 0$ at sound presentation) and frequency on the ordinate. Color represents mean power with warmer colors corresponding to an increased power and cooler colors representing decreased power compared to pre-stimulus baseline. **b.** Event-related power changes were separated into δ-, θ-, α-, β-, low γ- and high γ-frequency bands. Scale bars represent one oscillation cycle for the lowest frequency (longest duration cycle) in each band. Insets show traces on expanded time scale. Data are presented as mean power ± SEM. **c.** Time-frequency plots showing changes in phase locking factor (PLF) as a function of time and frequency. Color represents PLF with warmer colors corresponding to a higher PLF or lower circular variance in EEG phase across trials. **d.** PLF was separated into frequency bands. Data are presented as mean PLF ± SEM.

Nature Neuroscience: doi:10.1038/nn.2997

Figure S11

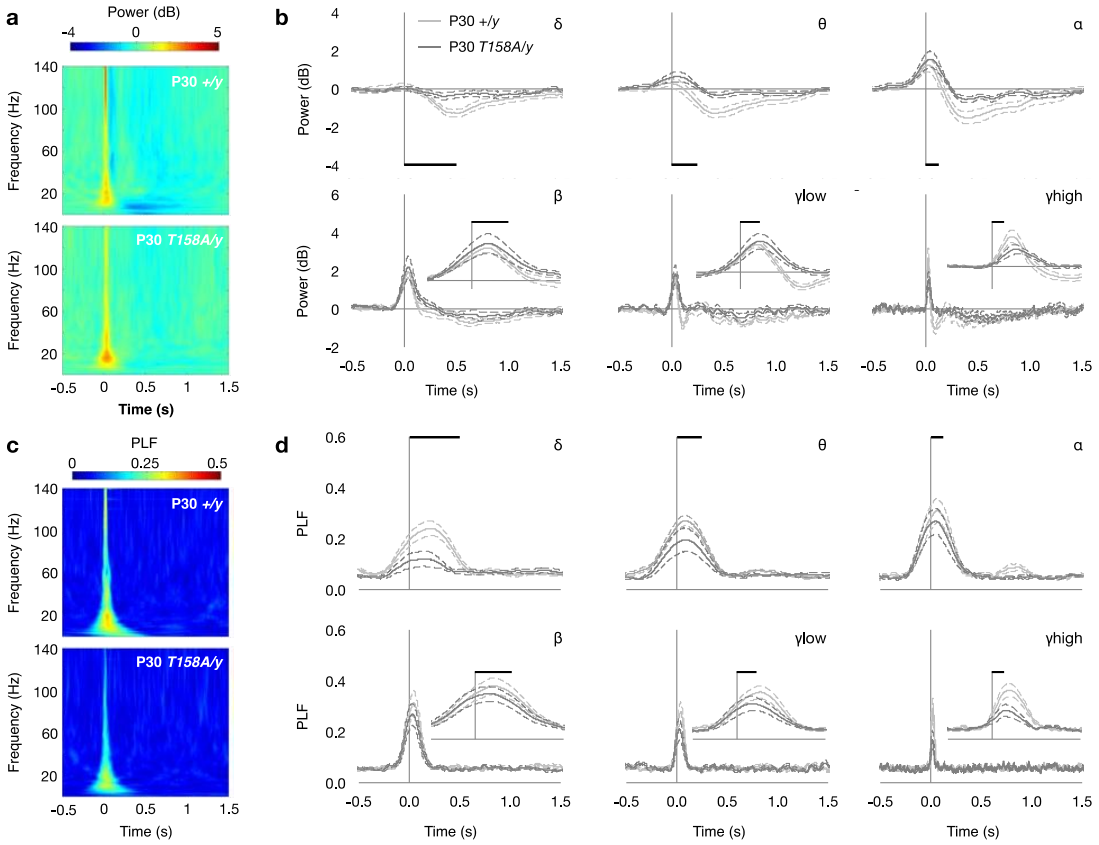

Supplementary Figure 11: Time-frequency analysis in P30 *Mecp2*$^{T158A/y}$ mice

a. Time-frequency plots showing event-related power in response to an 85-dB white noise clicks. Time is plotted on the abscissa (where *t = 0* at sound presentation) and frequency on the ordinate. Color represents mean power with warmer colors corresponding to an increased power and cooler colors representing decreased power compared to pre-stimulus baseline. **b.** Event-related power changes were separated into δ-, θ-, α-, β-, low γ- and high γ-frequency bands. Scale bars represent one oscillation cycle for the lowest frequency (longest duration cycle) in each band. Insets show traces on expanded time scale. Data are presented as mean power ± SEM. **c.** Changes in phase locking factor (PLF) as a function on time and frequency. Color represents PLF with warmer colors corresponding to a higher PLF or lower circular variance in EEG phase across trials. **d.** PLF was separated into frequency bands. Data are presented as mean PLF ± SEM.

Nature Neuroscience: doi:10.1038/nn.2997

Figure S12

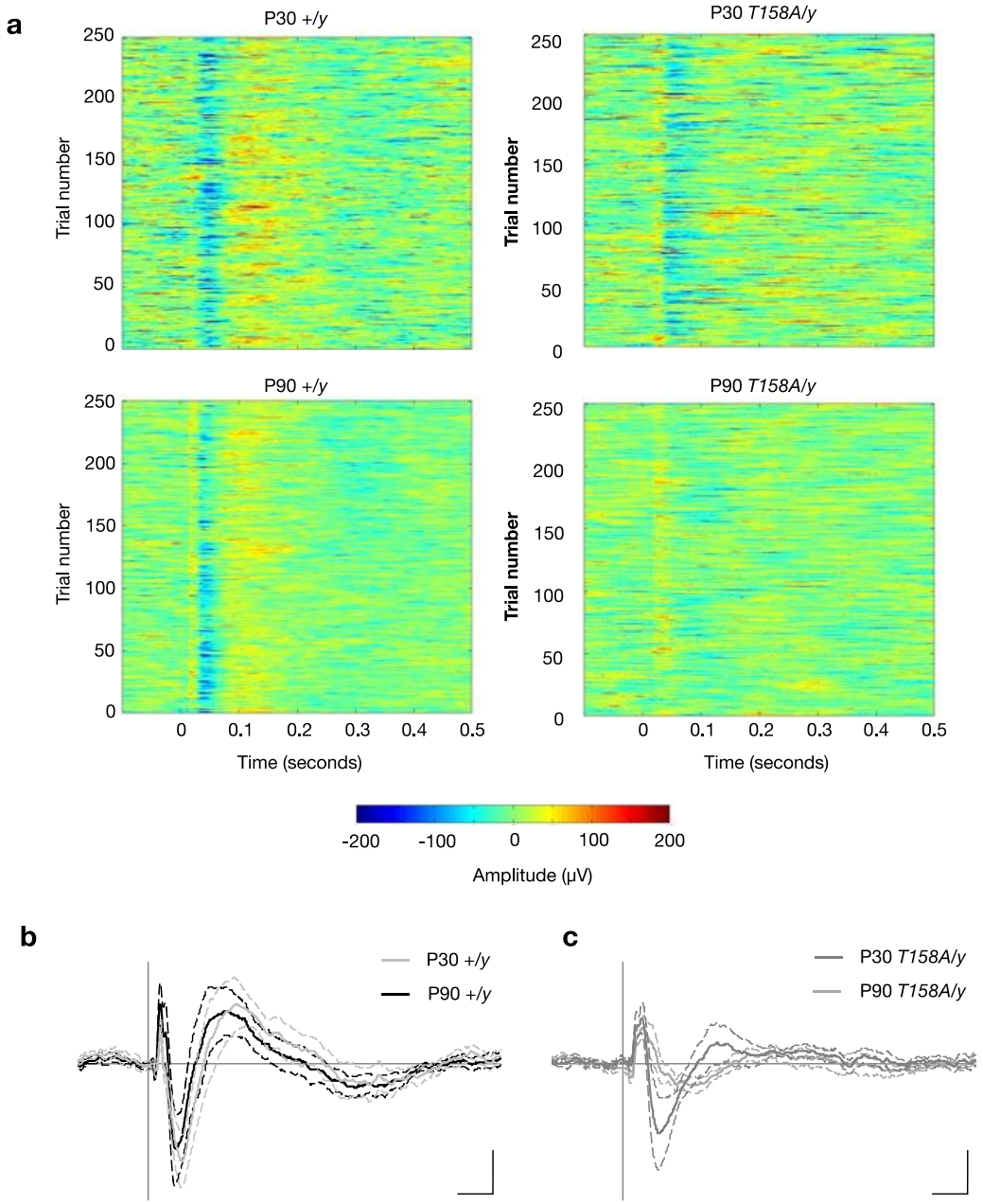

Supplementary Figure 12: Auditory-evoked ERPs in *Mecp2*$^{+/y}$ and *Mecp2*$^{T158A/y}$ mice

a. Heat maps showing ERPs recorded following presentation of 250 white-noise clicks (10 ms duration, 85-dB sound pressure, 4 second interstimulus intervals). Time is shown on the abscissa and trial number on the ordinate with the color representing EEG amplitude (μV). **b.** Grand average ERPs for *Mecp2*$^{+/y}$ mice at P30 and P90. Traces represent mean amplitude ± SEM. Scale bar corresponds to 50 ms (horizontal) and 20 μA (on vertical). **c.** Grand average ERPs for *Mecp2*$^{T158A/y}$ mice at P30 and P90. Traces represent mean amplitude ± SEM. Scale bar corresponds to 50 ms (horizontal) and 20 μA (on vertical).

Nature Neuroscience: doi:10.1038/nn.2997

Figure S13

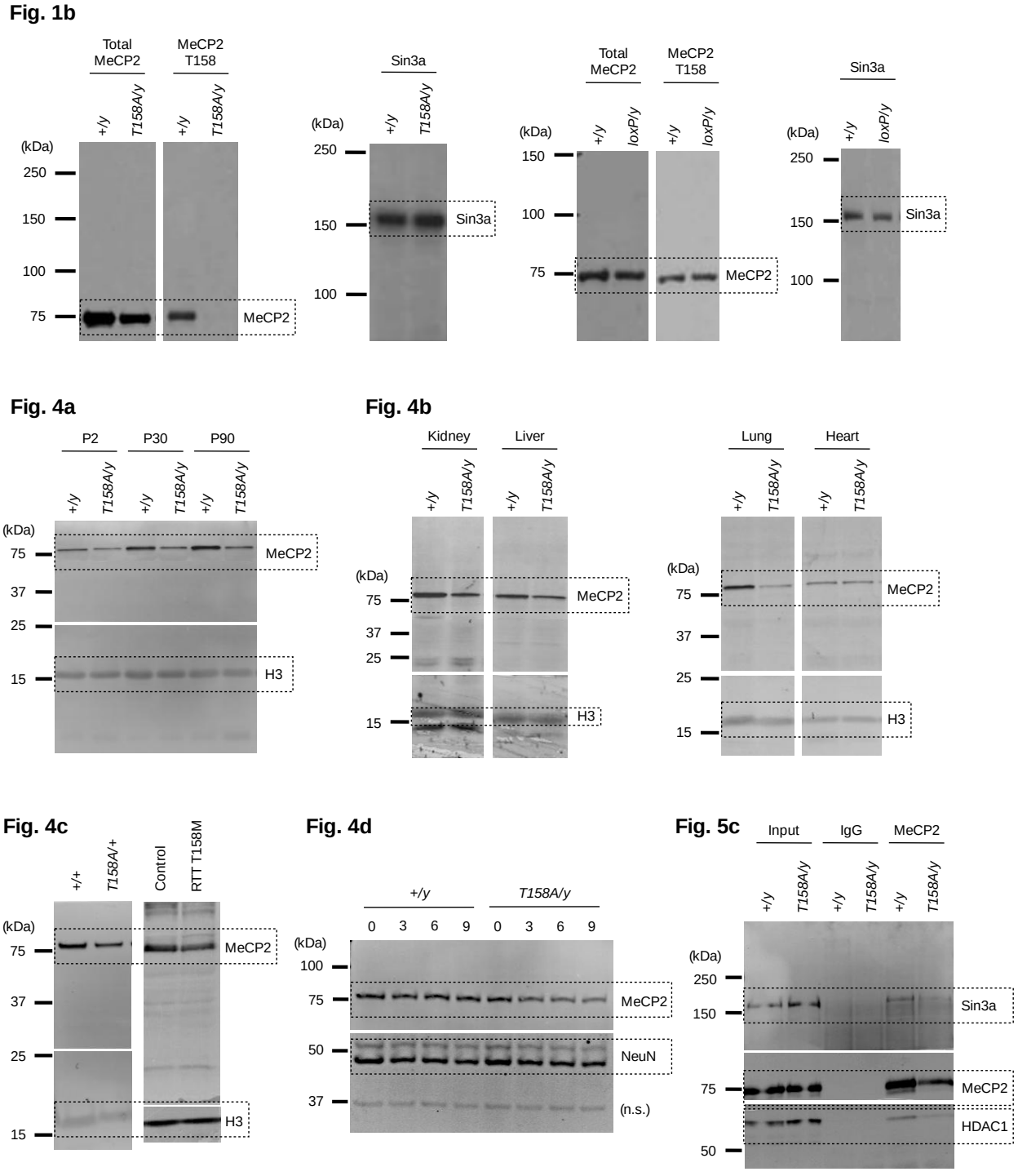

Supplementary Figure 13: Full-length pictures of the blots presented in the main figures. To examine proteins of interest on the same sample, blots in figures 4 and 5 were cut first and then probed with indicated antibodies.

Nature Neuroscience: doi:10.1038/nn.2997

Figure S14

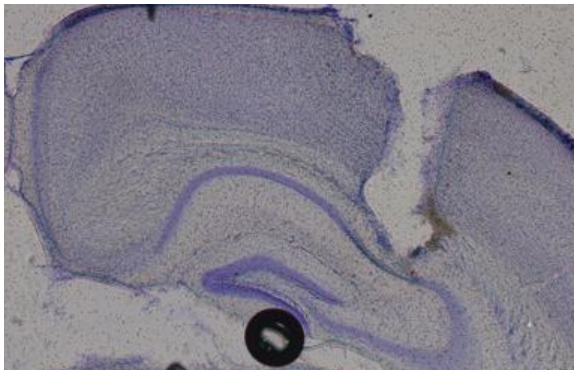

Supplementary Figure 14: EEG electrode placement in hippocampus

Representative 100 μm brain section with Nissl staining showing electrode placement in hippocampus.

Nature Neuroscience: doi:10.1038/nn.2997

Figure S15

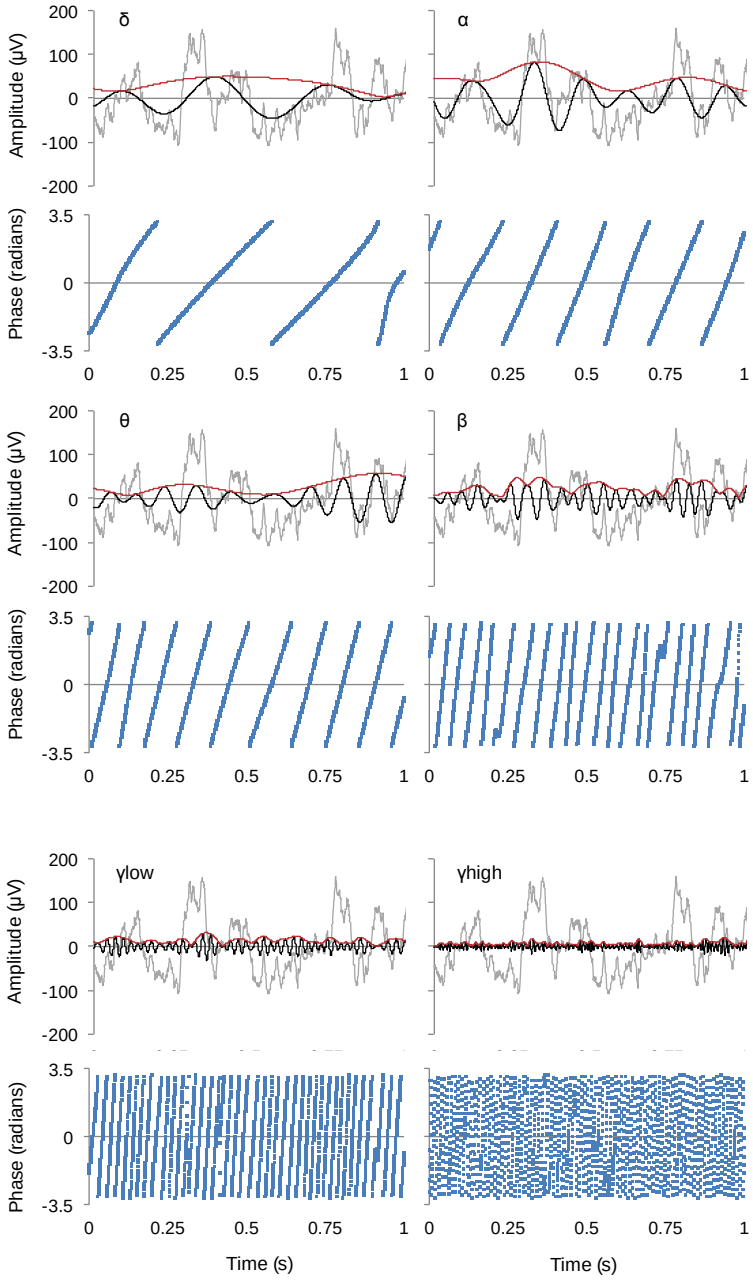

Supplementary Figure 15: EEG analysis using Hilbert transform

Time-frequency analysis was calculated using Hilbert transform to generate instantaneous amplitude and phase measurement. Traces show 1 second raw EEG trace in gray from P90 *Mecp2*$^{+/y}$ (WT) mice with the trace filtered at δ (2-4 Hz), θ (4-8 Hz), α (8-12 Hz), β (12-30 Hz), γlow (30-50 Hz) and γhigh (70-140 Hz) frequencies and shown in black. Amplitude envelope calculated from Hilbert transform is shown in red. Phase calculation is shown underneath with values expressed in radians.

Nature Neuroscience: doi:10.1038/nn.2997

Supplementary Video 1: Motor deficits in *Mecp2*$^{T158A/y}$ mice

Example video shows locomotor deficits in male *Mecp2*$^{+/y}$ (starts at bottom left), *Mecp2*$^{T158A/y}$ (starts at top right) and *Mecp2*$^{-/y}$ mice (starts at top left) at 11 weeks of age. Both *Mecp2*$^{T158A/y}$ and *Mecp2*$^{-/y}$ mice show decreased locomotor activity and aberrant gait with splaying of hind limbs upon movement.

Nature Neuroscience: doi:10.1038/nn.2997